Wilson, P.A., Lyle, M., and Firth, J.V. (Eds.)
Proceedings of the Ocean Drilling Program, Scientific Results Volume 199

21. Biogenic Sedimentation in the Eocene Equatorial Pacific—the Stuttering Greenhouse and Eocene Carbonate Compensation Depth[1]

Mitchell Lyle,[2] Annette Olivarez Lyle,[2] Jan Backman,[3] and Aradhna Tripati[4]

ABSTRACT

$CaCO_3$, C_{org}, and biogenic SiO_2 were measured in Eocene equatorial Pacific sediments from Sites 1218 and 1219, and bulk oxygen and carbon isotopes were measured on selected intervals from Site 1219. These data delineate a series of $CaCO_3$ events that first appeared at ~48 Ma and continued to the Eocene/Oligocene boundary. Each event lasted 1–2 m.y. and is separated from the next by a low $CaCO_3$ interval of a similar time span. The largest of these carbonate accumulation events (CAE-3) is in Magnetochron 18. It began at ~42.2 Ma, lasted until ~40.3 Ma, and was marked by higher than average productivity. The end of CAE-3 was abrupt and was associated with a large-scale carbon transfer to the oceans prior to warming of high-latitude regions. Changes in carbonate compensation depth associated with CAE excursions were small in the early part of the middle Eocene but increased to as much as 800 m by the late middle Eocene before decreasing into the late Eocene. Oxygen isotope data indicate that the carbonate events are associated with cooling conditions and may mark small glaciations in the Eocene.

[1] Lyle, M., Olivarez Lyle, A., Backman, J., and Tripati, A., 2005. Biogenic sedimentation in the Eocene equatorial Pacific—the stuttering greenhouse and Eocene carbonate compensation depth. *In* Wilson, P.A., Lyle, M., and Firth, J.V. (Eds.), *Proc. ODP, Sci. Results,* 199, 1–35 [Online]. Available from World Wide Web: <http://www-odp.tamu.edu/publications/199_SR/VOLUME/CHAPTERS/219.PDF>. [Cited YYYY-MM-DD]
[2] Center for Geophysical Investigation of the Shallow Subsurface, Boise State University, MS 1536, 1910 University Drive, Boise Idaho 83725, USA. Correspondence author: mlyle@cgiss.boisestate.edu
[3] Department of Geology and Geochemistry, Stockholm University, 106 91 Stockholm, Sweden.
[4] Department of Earth Sciences/Godwin Laboratory, University of Cambridge, Downing Street, Cambridge CB2 3EQ, United Kingdom.

Initial receipt: 29 April 2004
Acceptance: 11 March 2005
Web publication: 2 December 2005
Ms 199SR-219

INTRODUCTION

The Eocene, a 21 m.y. epoch of the Cenozoic, is well known for stable, warm climate conditions, but there is surprisingly little detailed information about paleoceanographic conditions that were a major part of the climate machine. Modeling studies and proxy data suggest that a significant contribution to warm conditions was provided by atmospheric CO_2 (Pearson and Palmer, 2000; Demicco et al., 2003; Shellito et al., 2003; Royer et al., 2004). Others have challenged this assertion, however (Veizer et al., 2000). One of the constraints on changes in atmospheric CO_2 is ocean pH—low ocean pH supports high atmospheric CO_2 (Royer et al., 2004), or, vice versa, maintenance of high atmospheric CO_2 drives ocean pH down (Caldeira and Wickett, 2003). Low ocean pH lowers the activity of CO_3^{2-} in seawater, causing higher net dissolution of $CaCO_3$ and smaller magnitudes of $CaCO_3$ burial in the deep ocean. The carbonate compensation depth (CCD) is thus an indicator of ocean pH because the depth-dependent increase in $CaCO_3$ dissolution favors preferential loss of carbonate from deeper ocean regions. Calcium content of the oceans probably changed during the Cenozoic (Hardie, 1996; Horita et al., 2002) and could also affect the CCD, but changes in the weathering cycles needed to change Ca are typically much slower than changes in the C system. The residence time of Ca relative to the carbon cycle (~10^6 yr residence time for Ca vs. 10^5 yr for C) (Broecker, 1971) is a rough indicator of the relative response times. Significant changes in ocean pH and atmospheric CO_2, if driven by changes in biogeochemical cycles, can happen much more rapidly (on the order of 10^3 yr), as is being shown by the modern anthropogenic CO_2 transient (Caldeira and Wickett, 2003) and the Paleocene/Eocene boundary event (Dickens et al., 1995, 1997; Thomas et al., 2002).

Ocean Drilling Program (ODP) Leg 199 is the first drilling transect across a major cog in the Eocene ocean-atmosphere climate system, the equatorial Pacific (Lyle, Wilson, Janecek, et al., 2002). The eastern equatorial Pacific, the Eocene paleoposition of the Leg 199 transect, has always been a major locus for insolation heating of the oceans and, therefore, a major factor in ocean heat balance (Huber and Caballero, 2003). In addition, the Pacific was volumetrically larger in the Eocene, composing roughly two-thirds of all the tropical oceans rather than the modern one-half.

In the modern oceans, the tropics are a major area where $CaCO_3$ is deposited. The tropics should also have been important in the Eocene as a locus of pelagic carbonate production, if not burial. However, previous drilling has shown that the CCD was shallow in the Eocene and radically deepened during the Eocene–Oligocene transition (van Andel, 1975; Berger et al., 1981; Delaney and Boyle, 1988; Peterson et al., 1992; Coxall et al., 2005) associated with the first major Antarctic glaciation, Oi-1 (Miller et al., 1991; Zachos et al., 2001). Deep Sea Drilling Project (DSDP) drilling also showed that there is a high temporal variability to $CaCO_3$ deposition in the Eocene tropics (van Andel, Heath, et al., 1973). The timing of this variability has not yet been well documented, nor are the processes well understood.

In this paper, we collected detailed data for two Leg 199 drill sites (Sites 1218 and 1219) and developed detailed biogenic sedimentation time series (see also **Olivarez Lyle and Lyle,** this volume). We explore how carbonate burial varied during a 12-m.y. interval in the middle and late

Eocene from ~46 Ma to the Eocene/Oligocene boundary (33.6 Ma), a period in which the CCD was extremely shallow and $CaCO_3$ burial in the deep ocean was low. We found long-period carbonate cycles in the equatorial Pacific sediments and link these cycles to initial Antarctic glaciations. We combined information from three drill sites (Sites 1218, 1219, and 1220) to study the change in the CCD and productivity for a critical 4-m.y. subinterval (42–38 Ma) for which we have overlapping records and found that the distribution of carbonate cannot be explained by depth-dependent dissolution in a one-dimensional ocean. Instead, we found a shallower CCD at the equator than at a paleoposition at 2°S, a situation reversed from modern conditions. The deeper off-equator CCD, which was probably caused by elevated carbonate production away from the equator, fits with Leg 199 observations of early Eocene $CaCO_3$ deposition (Rea and Lyle, 2005) north of the equator. Similarly, relatively high $CaCO_3$ deposition in the Antarctic region over the Eocene (Nelson and Cooke, 2001) suggests carbonate burial in the Pacific was organized in a different manner than in the Holocene.

We also found that the buildup of the largest of these carbonate accumulation events (CAEs), beginning at 41.5 Ma, was caused by increased production of carbonate. The appearance of $CaCO_3$ in the sediments is linked to polar glaciation. The end of CAE-3, the largest event, was caused by enhanced dissolution, with important implications for the carbon cycle.

SITE DESCRIPTIONS

During Leg 199, a transect was drilled across the Eocene equatorial region following 56-Ma crust, with one additional site located at the 40-Ma paleoequatorial position on 42-Ma crust (Lyle, Wilson, Janecek, et al., 2002) (Fig. **F1**). The primary objective of the drilling was to capture a latitudinal transect at the Paleocene/Eocene boundary. Nevertheless, the combination of sites on younger and older crust for the middle and late Eocene provided an opportunity to study the CCD after in detail 42 Ma.

Site 1218

Site 1218 (Fig. **F1;** Table **T1**) was sited at the 40-Ma equator to study middle Eocene equatorial processes and to provide a late Eocene to early Miocene record of paleoceanographic evolution of the tropical Pacific (Lyle, Wilson, Janecek, et al., 2002). One of the primary objectives of drilling at this site was to obtain a good quality record of the Eocene–Oligocene transition from "greenhouse" to "ice house" Earth conditions. Because of the shallow CCD, Eocene sediments from Site 1218 had relatively low carbonate compared to Oligocene sediments. The carbonate content of the 42- to 34-Ma sediments averages 40 wt% but ranges between 0 and 90 wt%. The lower Oligocene and Eocene sedimentary section was drilled with the extended core barrel (XCB) because burial had lithified sediments of this age and advanced piston coring (APC) was not possible. The sediments drilled with the XCB are thus more disturbed than the overlying lower Oligocene–Holocene APC-cored section. However, a complete sediment column was recovered to 41.2-Ma sediments (287 meters composite depth [mcd]), and only small gaps were uncored between 287 mcd and the 42-Ma basement (11 m deeper).

F1. Site map, p. 22.

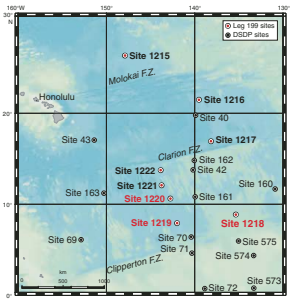

T1. C_{org}, $CaCO_3$, and opal, Site 1218, p. 30.

Site 1219

Site 1219 (Fig. F1; Table T2) was located ~4.6° south of the equator at the time of crust formation (54.5 Ma). At 42 Ma, it was located at ~2.2°S, and the site was carried northward across the equator at ~30 Ma by the Pacific plate. Because the Oligocene and Neogene sediments at Site 1219 were thinner than those at Site 1218, it was possible to APC core to a depth of 224.5 meters below seafloor (mbsf), or an age of ~48.9 Ma (H. Pälike, unpubl. data). The sediment column was completely drilled to a depth of ~245 mbsf (a basal age of ~54.5 Ma). Only one hole was drilled to basement and through the Eocene section because an APC core jammed in the drill bit as the Eocene/Oligocene boundary section was being drilled in Hole 1219B. The site was abandoned because we believed that we could drill a better section that also contained the Paleocene/Eocene boundary section farther north, nearer the paleoequator. Because Site 1219 was APC cored, it was possible to measure paleomagnetic vectors and determine a paleomagnetic chronostratigraphy to constrain age models within the Eocene. In addition, the similarity of sedimentation between Sites 1218 and 1219 made it possible to develop a precise stratigraphic correlation between the two sites and allowed the development of a common timescale (H. Pälike, unpubl. data). The Eocene sediment section is primarily radiolarian ooze, but intervals of carbonate deposition are present in the upper and middle Eocene sediments (see "Results," p. 8).

T2. C_{org}, $CaCO_3$, opal, and bulk ^{18}O, Site 1219, p. 31.

Site 1220

Site 1220 (Fig. F1) was located at the equator at 40 Ma but on deeper and older crust than at Site 1218. The basal sediment age is just slightly older than the Paleocene/Eocene boundary, or just older than 55 Ma. The sediment column is 200 m thick and was APC cored to a depth of 152 mbsf (46.3 Ma). The seafloor at Site 1220 is 200 m deeper than that at Site 1219, but the offset was mostly due to a thicker Oligocene and lower Miocene sediment section at Site 1219. The depth offset between the two sites at 40 Ma was 80 m. We expected to find carbonates within the same middle Eocene intervals noted at Site 1219 because Site 1220 was closer to the Eocene equator than Site 1219 and should have experienced higher biogenic sedimentation. We were surprised to discover that the entire middle and upper Eocene section of Site 1220 was barren of $CaCO_3$ (Lyle, Wilson, Janecek, et al., 2002).

Paleopositions

We calculated paleopositions reported in Tables T1 and T2 using the hotspot-Pacific plate motion model used in the Leg 199 *Initial Reports* volume (Lyle, Wilson, Janecek, et al., 2002; see the "Supplementary Materials" contents list). We checked this model against the best new piece of information from Leg 199—the crossing of the equator observed at Site 1219. Paleomagnetic inclination, magnetization intensity, and sedimentation rates all indicate that the equatorial crossing occurred when sediments at 130 mcd ± 10 m in the sediment column were deposited. This translates to an age of 29.5 Ma for the equatorial crossing, with a range between 29.0 and 30.4 Ma. The fixed-hotspot estimation predicts an equator crossing at the same time and thus appears to be adequate to estimate paleopositions in the central and eastern Pacific through the Eocene.

Sedimentation rate is highly dependent upon latitude and has a strong peak at the equator from the Oligocence to the Holocene because of biogenic deposition from the upwelling system (Murray et al., 1993; Pisias et al., 1995; Lyle, 2003; Rea and Lyle, 2005). Because of peak productivity and C_{org} particulate rain at the equator (Honjo et al., 1995), there should also be a minimum in magnetic intensity. Provided that iron-bearing minerals are uniformly supplied to sediments at a relatively low rate and that the C_{org} particulate rain is strongly dependent on proximity to the equator, magnetization should show a minimum at the equator (Karlin et al., 1987; Musgrave et al., 1993).

These indicators show that the position difference for the equatorial region from the Site 1219 lower Oligocene sediments compared to the fixed hotspot approximation estimate is <1°. Tarduno et al. (2003) showed that the Hawaiian hotspot moved significantly before 47 Ma but argue that the hotspot became fixed at about that time. Estimated positions by the fixed hotspot model before 47 Ma thus may be offset to the south of their actual position because of the overcompensated movement of the Pacific plate. The moving hotspot problem should have minimal effect on our estimated positions because we report sediments between the ages of 49 and 33 Ma. Moore et al. (2004) reached a similar conclusion about equatorial position based on sedimentation rate patterns from the entire DSDP and ODP set of drill sites, recalibrated using Leg 199 chronostratigraphy.

ANALYTICAL METHODS

Calcium Carbonate and Organic Carbon

Calcium carbonate and organic carbon were determined by coulometry at Boise State University (BSU; Idaho, USA) using a UIC, Inc. model CM-5012 CO_2 coulometer attached to our modified version of a CM-5120 combustion furnace. See **Olivarez Lyle and Lyle** (this volume) for special notes regarding the C_{org} analysis. Approximately 30–70 mg of dried, homogenized sediment sample was combusted in an ultra-high-purity oxygen (>99.994% O_2) atmosphere at 1000°C. The reported $CaCO_3$ data were calculated as the difference between two independent analyses of carbon from each sampled interval. First we measured the total carbon concentration of an untreated sediment sample, followed by a second analysis of a sample aliquot after pretreatment with 10% hydrochloric acid solution to dissolve solid $CaCO_3$. Inorganic carbon was calculated as the difference between the total carbon and the C_{org} fractions. The amount of $CaCO_3$ (in weight percent) is the product of inorganic carbon (in weight percent) and 8.33.

An additional set of samples was run for $CaCO_3$ at Stockholm University (Sweden) using a UIC coulometer with an acidification module. A subset of the Stockholm samples was also run at both laboratories, and results of the interlaboratory comparison showed no systematic differences between the two laboratories. The Stockholm samples (marked J. Backman) are interleaved with the BSU analyses in Tables **T1** and **T2.**

C_{org} was measured at BSU after the sample was pretreated with acid to remove carbonates. Approximately 70 mg of dried sample was placed inside a fused quartz combustion boat and then wetted with water and 10 drops of 10% HCl. The slurry was stirred and heated at ~110°C until sufficient solution evaporated to accommodate a second treatment

with the acid. After ~1 hr, samples were oven-dried and allowed to cool before analysis with the coulometer.

Accuracy was estimated by including two independent standards in each sample run, and precision was estimated by repeating the analyses of a subset of the unknown samples. As standards, we used a reagent-grade calcium carbonate or reagent-grade sucrose and an in-house standard, Midway, a marine sediment from the northeast Pacific Ocean. Precision of the unknowns was estimated by repeating the analysis of every fourth sample in the sample run. The average difference between the repeated samples is <0.01 wt% carbon. In general, samples were reanalyzed if the difference between the repeated analyses was ≥0.03 wt% C.

Biogenic Silica Analysis

Biogenic silica was measured by spectrophotometry after samples were digested in a 2-M KOH solution. The method is summarized below and discussed in great detail in Olivarez Lyle and Lyle (2002), a laboratory study designed to address the long-standing problem of measuring dissolution-resistant radiolarians in Eocene and Miocene marine sediments. There are two parts to the analytical problem: first, the widely used Mortlock and Froelich (1989) method, which employs a 2-M sodium carbonate bath, is ineffective at dissolving the Eocene radiolarians, as was shown for Leg 199 site survey sediments. Second, the pervasive assumption that clays are dissolved during the alkaline bath and therefore contribute significant amounts of dissolved silica to the result leads to an overestimation of the opal content of sediments. Olivarez Lyle and Lyle (2002) show that the harsher KOH treatment can successfully dissolve the biogenic silica component without compromising the analysis via clay dissolution.

Approximately 20–50 mg of dried sample was pretreated with hydrogen peroxide and hydrochloric acid to remove organic matter and carbonates. After this pretreatment, samples were rinsed, decanted, and oven-dried. Then, 20.0 mL of a 2-M KOH solution was added to samples in centrifuge tubes, including blanks, which were then capped, sonified, and weighed. Samples were placed in a covered shaking water bath and digested at 85°C. The samples in tubes then were centrifuged and allowed to cool for ~1 hr before analysis. Dissolved silica was measured by the heteropoly blue method using a Hach DR/4000 spectrophotometer following sample dilution with deionized, distilled water, following a standard procedure for low-range silica (Hach Method 8186).

Two standards were used for the opal analysis: a reagent grade dissolved silica standard (Hach 1106-49) and either the 1218C composite standard or the 1219A composite standard, both in-house sediment standards from Leg 199. These sediment standards were made by combining subsamples of equal mass from every sample we analyzed from each site. Therefore, the composite sediment standard should reflect all site-hole variation in biogenic silica and matrix materials. Summary statistics for the composite sediment standards are as follows: 1218C composite standard average = 32.2 ± 2.0 wt% SiO_2 (n = 87) and 1219A composite standard average = 56.3 ± 1.7 wt% SiO_2 (n = 52). In certain cases, a diatom ooze sediment standard was used from ODP Leg 178 Site 1098 (average = 31.2 ± 1.4 wt% SiO_2; n = 14) because an existing database using our laboratory method had been established (Olivarez Lyle and Lyle, 2002). Generally, every sample was analyzed twice and every fourth unknown sample was replicated in the same run (as samples in

separate tubes). Samples were reanalyzed in a later run if the difference between the repeated analyses exceeded ±8 wt% SiO_2. Note that reported biogenic silica data have not been corrected for structural water content, which can be as high as 15 wt% in radiolarians.

Bulk Carbonate Oxygen Isotope Analysis

We analyzed 109 samples from Site 1219 for bulk carbonate oxygen isotopes at Stockholm University. The samples were first run for $CaCO_3$, and samples that contained >10 wt% $CaCO_3$ were sent for analysis. The samples were dried and powdered, and then a 100- to 150-g sample was placed in a Kiel carbonate preparation device and analyzed on a Finnegan MAT mass spectrometer. Analytical precision is better than 0.1‰.

Mass Accumulation Rates

To account for differences in the mass of material preserved per unit time and the differential compaction of downcore intervals, we converted all linear sedimentation rate data to mass accumulation rates (MARs) for all intervals. MAR is defined as the product of the linear sedimentation rate (LSR; length/time) and the dry bulk density (DBD; mass/volume) and has units of [mass/(unit area × unit time)]. DBD is related to wet bulk density (WBD) by the following equation:

$$DBD = WBD - P(\rho_{H2O}),$$

where P is pore fraction and ρ_{H2O} is the water density.

Because the multisensor track (MST) measures wet bulk density at the centimeter scale, there are ~2 orders of magnitude more data for WBD than DBD. We took advantage of the added resolution of the WBD data by estimating DBD from WBD. The shipboard moisture and density measurements of these parameters were used to define linear regression equations which relate DBD as a function of WBD. Subsequently, the appropriate equation, based on a relatively low resolution of samples, was applied to the shipboard gamma ray attenuation (GRA) wet bulk density measurements, spaced every 2 cm for our samples, to generate a high-resolution DBD data set. We used the stacked WBD data assembled by H. Pälike (unpubl. data) as the basis for the DBD data set.

For each site, correlation coefficients were very high (r = 0.997) for the low-resolution linear regression generated when all of the data were utilized (i.e., all lithologic units) (**Olivarez Lyle and Lyle,** this volume). However, better correlations, along with different regression equations, were obtained when the regressions were generated based on major lithologic units identified for each drill site. Ultimately, we decided to use the regression equations based on lithology to predict the DBD value (and resulting MAR) rather than using a single equation for each site. This decision is justified by the magnitude of the differences in the predicted DBD values that resulted from the lithology-based equations. The difference was particularly important for the Eocene radiolarian ooze and clay section. DBD calculated using the regression based upon lithology was significantly closer to the measured DBD and systematically 7% higher than DBD calculated by the site average regression.

RESULTS

Our analyses are presented in Table T1 for Site 1218 and Table T2 for Site 1219. We find a factor of 2–4 variability in opal and C_{org} at each site but order of magnitude changes in $CaCO_3$. We observe significant production changes at each site, particularly in the time interval between 38 and 42 Ma, with large additional changes in $CaCO_3$ superimposed. Figure F2 shows the 33- to 55-Ma time series of $CaCO_3$, C_{org} (expressed on a carbonate-free basis), and biogenic SiO_2 (carbonate-free) at Sites 1218 and 1219. C_{org} and biogenic SiO_2 are shown on a carbonate-free basis to remove the dilution effects of carbonate on the other biogenic time series. A better way to remove these dilution problems is to convert percentage data to mass accumulation rates (Fig. F3). Deposition of particulate material at the seafloor to generate the sediment column is unlike adding solutes to a dilute solution; on the contrary, addition or removal of any one sedimentary component during deposition changes the percentage of all others present. In contrast, dilution effects among solutes in solution are usually negligible because the concentration of solutes is extremely small relative to the solvent. MAR time series better show the real variation in sediment deposition than percentage data, provided that the age model is reasonably accurate.

The age models we use are the best presently available for the Eocene. Age models for both Sites 1218 and 1219 have been orbitally tuned and intercorrelated to the base of Site 1218 (42 Ma) (H. Pälike, unpubl. data). Because we were able to APC core the Eocene section at Sites 1219 and 1220 and reliably measure paleomagnetic reversals, we were able to base the middle Eocene (42–50 Ma) age model on paleomagnetic chronostratigraphy (Cande and Kent, 1992, 1995). Age models are less reliable for the lower Eocene section below the ubiquitous chert layers near the lower/middle Eocene boundary; for this section there are no improvements on age control beyond the shipboard work reported in the Leg 199 *Initial Reports* volume (Lyle, Wilson, Janecek, et al., 2002).

$CaCO_3$

$CaCO_3$ time profiles (both weight percent and MAR) illuminate a series of events in the middle and late Eocene. The ages, magnetochrons, and revised meters composite depths (rmcd) of these events are displayed in Table T3 using the chronostratigraphy by H. Pälike (unpubl. data). Carbonate events occur about every 2 m.y. in the middle–late Eocene up to the Eocene–Oligocene transition. We refer to these as carbonate accumulation events (Table T3). The largest of these events (CAE-3) is between 40.5 and 41.5 Ma, mostly in Magnetochron C18r. We have evidence that these carbonate events are associated with polar cool conditions (see below) and are weaker analogs to the Oi-1 event of the Eocene–Oligocene transition (Coxall et al., 2005). The largest of these CAE events (CAE-3) reaches its maximum about half a million years after the warm Middle Eocene Climate Optimum (MECO) event reported by Bohaty and Zachos (2003), which ended at ~41.5 Ma. The end of CAE-3 was caused by a relatively slow decrease in productivity upon which a rapid shallowing of the CCD is superimposed, indicative of a large C_{org} transfer to ocean waters from an external reservoir (see below).

F2. $CaCO_3$, biogenic SiO_2, and C_{org}, p. 23.

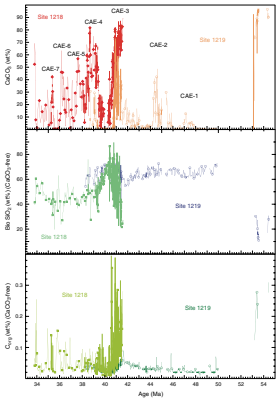

F3. $CaCO_3$, biogenic SiO_2, and C_{org} MARs, p. 24.

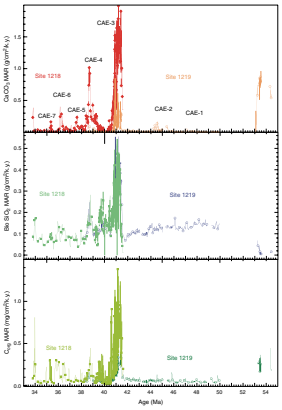

T3. Carbonate accumulation events, p. 32.

Site 1219 displays a basal carbonate section typical of pelagic sediments on cooling and deepening ocean crust. Basal carbonates disappear by 53 Ma (Figs. F2, F3). The section between 53 and 50 Ma was not recovered, but a continuously cored, though not complete, section of the younger sediments was recovered. We analyzed the sediment section between 50 and 38 Ma in detail but did not analyze the upper Eocene section. Based on shipboard surveys for nannofossils, the two upper Eocene cores (199-1219A-18H and 19H) were barren of nannofossils except at the very base of Core 19H (Lyle, Wilson, Janecek, et al., 2002).

The events older than 42 Ma are best delineated in the $CaCO_3$ weight percent record (Fig. F2) rather than MAR (Fig. F3) because nonlinearities in percentage expand the low part of the percentage scale relative to MAR. The events generally have multiple peaks of $CaCO_3$ deposition, and we can demonstrate orbital cyclicity of $CaCO_3$ MAR in CAE-3, the best resolved event.

Site 1218, because of its younger basal age, contains only the events from CAE-3 to CAE-7. The magnitude of the CAEs thus gradually increases from 50 Ma up to CAE-3 (41.5–40.5 Ma) and decreases afterward.

Biogenic SiO_2 and C_{org}

C_{org} and biogenic SiO_2 vary significantly over the middle and late Eocene, but the magnitude of this variation is significantly smaller than that of the $CaCO_3$ variation. It appears that production may be an important factor to cause a carbonate accumulation event but that changes in carbonate dissolution magnify the $CaCO_3$ signal relative to the other biogenic components. Because high bulk MAR generally coincides with high carbonate intervals at Sites 1218 and 1219, there is a general similarity between the carbonate-free and MAR time series (Figs. F2, F3). Nevertheless, it is clear that there were distinctive styles of deposition in the middle and late Eocene (42–38 Ma) relative to modern depositional processes. **Olivarez Lyle and Lyle** (this volume) explore the productivity issues in detail. They note that much more of the C_{org} rain must have been recycled in the water column or surface sediments in the Eocene relative to the Holocene. In this paper we will briefly describe these time series and their relationship to the $CaCO_3$ record.

The early Eocene at Site 1219 (54.5–53 Ma) has relatively high C_{org} MAR but low biogenic SiO_2 MAR (Fig. F3). Because of the lack of good age control in this interval, we note only that the low opal content in the early Eocene is distinctive of the interval, consistent with similar work on the early Eocene section from Site 1221 (**Murphy et al.,** this volume), and also consistent with the difficulty in obtaining radiolarians for biostratigraphic studies from this interval. (T.C. Moore Jr., pers. comm., 2002).

For whatever reason, the early Eocene did not support conditions for radiolarians to grow and prosper. Except for certain distinctive intervals, essentially all the biogenic SiO_2 found in Leg 199 samples is derived from radiolarians. The most prominent of these diatom intervals occurs at the top of CAE-3, where the biogenic silica fraction is >50% diatoms. Diatoms never compose >5% of the total biogenic SiO_2 fraction in the rest of the Eocene based on smear slides (Lyle, Wilson, Janecek, et al., 2002).

The Eocene interval (50–34 Ma) at Sites 1218 and 1219 is marked by a long-term background trend in which biogenic SiO_2 MAR decreased

by about a factor of 2, from ~0.14 to 0.07 g/cm²/k.y. (Fig. F3). We interpret this to indicate a trend toward lower productivity from the beginning of the middle Eocene to the end of the Eocene. There is no long-term trend in the C_{org} MAR profile. A middle Eocene interval (42–38 Ma) of variable but much higher deposition is the most prominent feature in the Eocene records, coinciding with CAE-3 and CAE-4. We observe little response in C_{org} or biogenic SiO_2 MAR profiles across CAE-1 and CAE-2, possibly because there was not a strong change in productivity associated with these events.

The magnitude of biogenic SiO_2 MAR is comparable at both drill sites, within events as well as in the background intervals between events (Fig. F3). However, C_{org} MAR tends to be higher in the more carbonate rich sediments of Site 1218 relative to Site 1219 (Fig. F3). Site 1218 was significantly closer to the equator at ~40 Ma (Site 1218 = 0° paleolatitude vs. Site 1219 = 2°S), so higher MAR at Site 1218 might be expected at this time from differences in productivity. However, preservation of C_{org} is linked to oxygen exposure time (Hartnett and Devol, 2003), and the higher sedimentation rates at Site 1218 relative to Site 1219 may be the most important factor in the difference between the two sites. In the late Eocene, the two sites were roughly equal distances north and south of the equatorial region and the offset between sites should have disappeared. Unfortunately, we did not analyze C_{org} beyond 38 Ma at Site 1219 because of the lack of $CaCO_3$.

The middle Eocene interval of high but variable biogenic SiO_2 and C_{org} MARs overlaps the CAE-3 and CAE-4 carbonate events, but the interval of low $CaCO_3$ between CAE-3 and CAE-4 is relatively high in C_{org} MAR and biogenic SiO_2 MAR compared to the interval before CAE-3 or after CAE-5 (Fig. F4). The loss of $CaCO_3$ was disproportionate to the drop in MAR of other biogenic sedimentary components between CAE-3 and CAE-4. In other words, the C_{org} and biogenic SiO_2 MAR time series indicate that the sudden drop in $CaCO_3$ cannot be ascribed to a drop in production alone but must represent a major increase in $CaCO_3$ dissolution as well.

Estimating the Carbonate Compensation Depth

The CCD is defined as the shallowest depth at which the particulate rain of $CaCO_3$ is entirely dissolved before burial or, in other words, the shallowest depth at which $CaCO_3$ disappears from sediments. The location of the CCD can strongly constrain ocean carbon cycles because it depends on balancing carbonate production in the surface ocean and dissolution caused by ocean carbon chemistry in the abyss (Berger et al., 1976). Typically, $CaCO_3$ weight percent is used to estimate the CCD. However, the strong nonlinearities of percentage with respect to flux (Fig. F5) make CCD estimates based on percentage poor. Instead, $CaCO_3$ MAR should be used because the effects of dilution are factored out by MAR.

An example of the strong nonlinearity in weight percent data is shown in Figure F5. A hypothetical sediment composed of 90 wt% $CaCO_3$ and 10% clay (which is inert) is subjected to a linearly increasing dissolution gradient. About 80% of the $CaCO_3$ particulate rain must be dissolved to change carbonate from 90 to 65 wt%. The problem is even more acute if the secondary component in the sediment is also subject to dissolution, as is the case in equatorial Pacific sediments. Biogenic silica is typically the second most abundant sedimentary compo-

F4. Detail of interval from 43 to 37 Ma, p. 25.

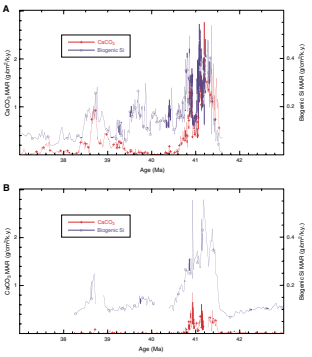

F5. CCD change estimated using percentages vs. $CaCO_3$ MAR, p. 26.

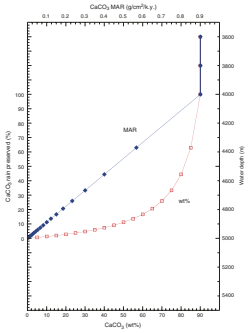

nent in the equatorial Pacific, and it dissolves readily (Archer et al., 1993). If both the carbonate and residual fractions of the sediment dissolve at similar rates, huge amounts of $CaCO_3$ dissolution may occur with little or no change in $CaCO_3$ weight percent. The use of $CaCO_3$ MAR eliminates the nonlinearity problem. Both the change in sediment composition and the change in mass are monitored with MAR. Provided that a common age model is used for sites from different water depths, a MAR-estimated CCD will be accurate even if the age model used to estimate MAR is wrong. Although the estimated absolute flux would be more inaccurate with a poor age model, the change in MAR with depth remains accurate because the mass change over the same time interval is being compared.

The MAR estimate of CCD can have errors because the CCD formulation assumes that the mass of $CaCO_3$ particulate rain is the same at all sites. One must therefore evaluate whether the vertical rain and any horizontal sediment focusing appear to be the same at different sites in order to test the validity of the CCD estimate.

CCD Changes in the Eocene Tropical Pacific

We used Sites 1218, 1219, and 1220 to estimate the CCD in the tropical Pacific. The time series for biogenic sediments are shown in Figures **F2, F3,** and **F4** for Sites 1218 and 1219 and provide the basis for detailed studies. We did not run new analyses on Site 1220 sediments but instead used shipboard data. The entire middle to upper Eocene section at Site 1220 is barren of carbonate, as evidenced by extensive unsuccessful searches for nannofossils for biostratigraphy. No new stratigraphic data for Site 1220 are available to us to refine the age model. Nevertheless, the data available suggest that Site 1220 biogenic SiO_2 MAR was similar to that at Sites 1218 and 1219, though perhaps lower. To the first order, the data at Site 1220 show the same trends in SiO_2 MAR with time. Thus, Site 1220 can help define the CCD as well, since it is 80–100 m deeper than Site 1219 throughout the Eocene (Table **T4**).

The $CaCO_3$ MAR data reported in Table **T4** were interpolated from our original data set (Tables **T1, T2**) to 0.02-m.y. spacing and then averaged over 0.1-m.y. increments. The CCDs shown in bold on Table **T4** are linear extrapolations from combined Site 1218 and 1219 data and are more robust than the other data. The data shown in italics represent extrapolations of the CCD assuming a decrease of roughly 0.001 g $CaCO_3/cm^2$/k.y. per additional meter of water depth near the CCD. This estimate, although not very accurate, allows us to better identify very large shifts in $CaCO_3$ MAR that occurred as the CCD passes one of the sites. In addition, this estimation allowed us to make some estimate, however poor, of the intervals covered by only one of the prime sites (Sites 1218 and 1219). Ideally, additional sites should be drilled to constrain CCD changes more fully.

For CAE-4 (39.3–38.6 Ma) (Table **T3**), estimates of the CCD are consistent among Sites 1218, 1219, and 1220, where we have more than one site with carbonate. Extrapolations from Sites 1218 and 1219 estimate that the CCD should be, within error, shallower than the depth of Site 1220 for certain of the CAE intervals. No $CaCO_3$ was preserved at Site 1220 throughout the middle and upper Eocene, however. During CAE-3 (42.2–40.3 Ma), the CCD estimated by the 1218–1219 pair is significantly deeper than the paleodepth of Site 1220, which has no $CaCO_3$. The overshoots deeper than Site 1220 average 100 m but reach 400 m at the peak of CAE-3 between 41 and 40.9 Ma. They indicate that

T4. Changes in carbonate compensation depth, p. 33.

at least part of the CCD estimate is caused by differential $CaCO_3$ rain between sites or that Site 1220 preferentially lost sediment flux relative to the other two sites.

Figure F6 illustrates the general situation for CAE-3. We expect, assuming the present provides a key to the past, that the two sites on the equator (1218 and 1220) should have similar $CaCO_3$ production and should best define the CCD. If Sites 1218 and 1220 are used to define the CCD, ~60% of the MAR at Site 1219 has to be excess (i.e., caused by sediment focusing at Site 1219 or by higher off-equatorial $CaCO_3$ production and burial at Site 1219 relative to Site 1220). We suggest that the excess may be due to higher $CaCO_3$ production at Site 1219 relative to Site 1220. Because Sites 1219 and 1218 have similar biogenic SiO_2 MAR, a more conservative measure of productivity, they are the best pair to use to estimate CCD. Even with the uncertainties, the CCD during CAE-3 gradually increased by ~600 m between 43.5 and 41 Ma and abruptly shallowed by at least 800 m between 40.8 and 40.7 Ma.

The disparity between CCD estimates from Sites 1220 and 1219 illustrates the sensitivity of the CCD to differences in $CaCO_3$ production and sedimentation. We determined that the Site 1218–1219 pair gives a better CCD estimate because the biogenic SiO_2 MAR at each site is nearly the same over the intervals for which we have common data (Fig. F3). Because biogenic SiO_2 was not measured at Site 1220, we cannot compare Site 1220 to the other two sites in detail. If we use the magnetic anomalies at Site 1220 and assume an average of 70 wt% biogenic SiO_2 in the sediments, biogenic SiO_2 MAR has a pattern similar to but somewhat lower than the average from Sites 1218 and 1219. Because the original $CaCO_3$ rain should be proportional to the rain of other biogenic components out of surface waters, these data indicate that initial $CaCO_3$ deposition at Site 1220 was generally somewhat lower than at the other two sites and the CCD estimate using Site 1220 should be skewed shallow.

The difference in CCD estimated by the Site 1218–1219 pair vs. the Site 1218–1220 pair appears to be more than a local difference caused by sedimentation. No site on the 56-Ma transect north of Site 1219 (Sites 1220, 1221, 1217, 1216, or 1215) contained any $CaCO_3$ in its middle and upper Eocene sections. There appears to be strong gradients in $CaCO_3$ production in the Eocene both longitudinally and latitudinally. We also found, for example, that $CaCO_3$ in lower Eocene sediments was better preserved away from the equator rather than near it (Lyle, Wilson, Janecek, et al., 2002).

F6. CCD estimate based on Sites 1218, 1219, and 1220 over CAE-3, p. 27.

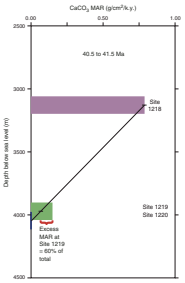

Oxygen Isotopes

A set of samples from Site 1219 with $CaCO_3$ contents >10 wt% was run for bulk oxygen isotope content at Stockholm University to test the hypothesis that the CAEs are indicators of Eocene polar glaciation (Fig. F7). This hypothesis derives from the rapid deepening of the CCD at the Eocene–Oligocene transition (Lyle, Wilson, Janecek, et al., 2002), now shown to be associated with the Oi-1 glaciation (Coxall et al., 2005). A second set of samples from CAE-3 at Site 1218 was analyzed for oxygen and carbon isotopes including bulk carbonate, benthic foraminifers, and planktonic foraminifers to study both surface and deepwater variations (Tripati et al., 2005). Heavier oxygen isotopes in bulk carbonate should indicate either a local cooling of surface waters (because bulk carbonate is primarily of nannofossil origin) or a whole-ocean change

F7. Bulk oxygen isotopes and $CaCO_3$, p. 28.

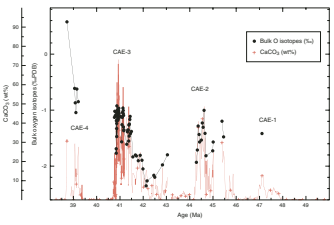

in oxygen isotope composition caused by the withdrawal of $\delta^{16}O$ into continental ice sheets.

Limiting bulk oxygen isotope analysis to Site 1219 samples containing >10 wt% $CaCO_3$ results in data that represent only the CAE events (Fig. F7). Analysis of these CAE samples revealed differences between the carbonate events. The most striking of these is that CAE-4 appears to be offset toward significantly heavier oxygen isotope values for equivalent $CaCO_3$ relative to the earlier CAE events measured, perhaps associated with the long-term isotope trend toward enrichment in $\delta^{18}O$ noted for the Eocene oceans (Zachos et al., 2001). It would be worthwhile to pursue these isotopic variations in a better preserved record elsewhere to differentiate between trends and events.

Within carbonate events (e.g., CAE-2 and CAE-3) there is a general correlation between heavy oxygen isotopes and high $CaCO_3$. Within CAE-3 there is also a tendency toward heavier oxygen isotope values as the event progressed. The lightest isotopic values are found at the beginning of CAE-3 (~42 Ma), and the isotopic values increase as the $CaCO_3$ content increases to 41 Ma. At the end of CAE-3, bulk oxygen isotopes at Site 1219 do not drop as fast as $CaCO_3$ values do.

These results mirror the isotope excursions observed at Site 1218. The oxygen isotope shift to lighter values is distinctly younger than the initial loss of $CaCO_3$, both in bulk carbonate isotopes as well as in benthic foraminiferal oxygen isotopes, as shown in Figure F8A. The first drop in $CaCO_3$ MAR occurred at 41 Ma, whereas oxygen isotope values lighten only after 40.7 Ma. The isotopic data shown in Figure F8 are confined to one core from one hole (Core 199-1218C-21X), so we know that the rapid changes we observe are not caused by an error in the sampling splice. The benthic foraminiferal isotope results thus implicate the high latitudes as the source of the signal because both of the causal mechanisms for oxygen isotope variation (ice and temperature) are set in high latitudes.

Although the oxygen isotopes do not align with the drop in $CaCO_3$ MAR, the first major drop in $CaCO_3$ coincides with an apparent 0.5‰ carbon isotope event in the deep water (Fig. F8B). Unfortunately, the base of this event is at the base of the studied core, so is as yet poorly defined. Tripati et al. (2005) more fully discuss the implications of these stable isotope records. We observe that high $\delta^{18}O$ correlates with high $CaCO_3$ and supports the link between increased carbonate burial at the equator and global cooling. The failure of glacial events to maintain themselves prior to the Eocene/Oligocene boundary suggests that strong negative feedbacks stabilized warm conditions in the Eocene but that this stabilization failed at the Eocene/Oligocene boundary.

F8. Oxygen and carbon isotope records, p. 29.

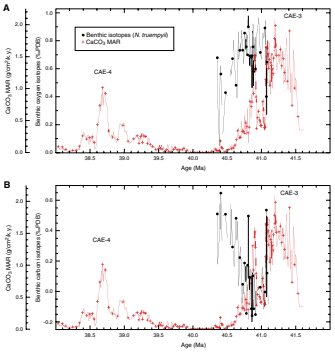

DISCUSSION

The different response of $CaCO_3$ compared to the other biogenic components of the Eocene sediment section is strong evidence of significant changes in ocean carbon chemistry over relatively short periods of time. We investigated change in the CCD between 38 and 41.6 Ma (base of Site 1218) in detail. We found that production of $CaCO_3$ was an important factor in deepening the CCD during CAE-3 but that dissolution was the most important factor ending CAE-3 at ~40.5 Ma. CAE-3 and CAE-4 are actually part of a single high-productivity interval divided by an interval of high $CaCO_3$ dissolution (Fig. F4). The dissolution between the events coincides with a major $\delta^{13}C$ anomaly followed

by warming conditions at the poles, as indicated by oxygen isotopes. The increases of $CaCO_3$ MAR and biogenic SiO_2 MAR were about equivalent at the start of CAE-3, and the CCD deepened relatively slowly. At the end of CAE-3, the CCD dropped abruptly by more than 500 m in 100 k.y. The decrease in deposition of other biogenic components occurred much more slowly and indicates that dissolution amplified the loss of $CaCO_3$ relative to biogenic Si and C_{org}. The total CCD shallowing from the peak of CAE-3 deposition at 41 Ma to the CCD minimum between 40.5 and 40.0 Ma is at least 800 m, about two-thirds the size but in the opposite sense as the CCD change at the Eocene–Oligocene transition.

CCD Changes Associated with CAE-3

The initiation of CAE-3 coincided with the end of the MECO event, just before 42 Ma (Bohaty and Zachos, 2003). Low levels of $CaCO_3$ were deposited during the MECO interval at Site 1219, so the equatorial Pacific CCD was relatively deep for the Eocene during the MECO event. We estimate that the CCD was probably in the range of 3900–4000 m then, slightly deeper than the paleodepth of Site 1219 at that time (Table T4). Because biogenic SiO_2 MAR increased by a factor of 4 at the start of CAE-3 and the CCD prior to the event was relatively deep, it is clear that a major factor in the $CaCO_3$ event was increased production of $CaCO_3$ in a productivity event.

$CaCO_3$ MAR increases after 42 Ma are also linked with a strong increase in $\delta^{18}O$ of bulk $CaCO_3$ (Fig. F7). The oxygen isotope increase of 1.2‰ was divided into two steps, roughly half before 41.5 Ma and half afterward. The total event thus involved either ~6°C cooling of surface waters or ~120 m of sea level change caused by ice growth or a combination of the two. The first step coincides with the beginning of CAE-3. Benthic oxygen isotopes (Fig. F8A) from Site 1218 and the bulk oxygen isotope record from Site 1219 show that the end of the event began while oxygen isotopes remained heavy. Significant loss of $CaCO_3$ thus began prior to a sea level rise associated with deglaciation.

The CCD minimum between CAE-3 and CAE-4 is one of the most extreme minima in the record. Biogenic SiO_2 MAR remains high over the interval, ~50% higher than the background biogenic SiO_2 MAR, so we expected that $CaCO_3$ MAR should have been ~0.2–0.4 g $CaCO_3/cm^2/k.y.$ if the dissolution rate remained constant. Instead, all $CaCO_3$ was dissolved. A primary cause of the $CaCO_3$ minimum must be changes in the carbon system within the ocean, making deep waters much more corrosive to solid $CaCO_3$. Figure F8B shows how the first disappearance of $CaCO_3$ between CAE-3 and CAE-4 apparently coincided with a large $\delta^{13}C$ minimum. The final disappearance of $CaCO_3$ coincided with the appearance of lighter oxygen isotopes, indicating warming and probably ice melting as well. The $\delta^{13}C$ minimum, if further work confirms its existence, should mark a large new addition of an isotopically light C_{org} reservoir to the oceans (e.g., additional C_{org} from the continents or a methane release), which would cause warming and increased carbonate dissolution in the oceans. Expansion of shallow seas from glacial melting may have further trapped $CaCO_3$ on the shelf regions and driven the pelagic CCD to extremely shallow depths. For a time near 40 Ma, the CCD rose above the level of Site 1218, or to a depth shallower than ~3250 m. Feedback within the carbon cycle thus ended the develop-

ment of ice sheets in Antarctica in the middle Eocene and returned the Eocene to warm conditions.

What Caused the CCD Change?

We documented that there were significant CCD changes in the equatorial Pacific through the middle and late Eocene and showed that the CCD changes are linked to long-term cooling events lasting as long as 2 m.y. We also showed that at least one of these events (CAE-3) was coincident with high-latitude cooling, implying that the CAEs mark glacial periods within the Eocene.

We suggest the cause of these events and their demise was a result of interesting dynamics between different carbon reservoirs in the carbon cycle interacting with climate. The evidence we have amassed suggests an interplay between pelagic carbonate production and changes in carbon reservoirs either internal or external to the ocean. We also note that the CAEs are sufficiently long that changes in the major cation content of the oceans could also have played a role in their evolution but not in their sudden appearance or disappearance.

Rapid changes in the equatorial Pacific CCD can be driven by any or all of several factors:

1. Shifting $CaCO_3$ depocenters from the deep ocean to shelves and shallow seas;
2. Shifting pelagic $CaCO_3$ production from regions outside the equator to the equatorial region; or
3. Changes in the dissolved inorganic carbon (DIC) content of the oceans relative to the net weathering flux of anions and cations.

Shifting $CaCO_3$ burial, either to shelf and shallow seas or from one region of the deep ocean to another, affects the CCD by changing the locus where weathering inputs are balanced. It is not important to the oceanic carbon cycle where the balance occurs. However, moving the locus of $CaCO_3$ deposition from the deep ocean to the shelf regions results in a shallow CCD because the total DIC of the oceans drops, CO_3^{2-} activity drops, and more $CaCO_3$ dissolves at shallower depths. The result is that the increased shallow $CaCO_3$ burial results in lower pelagic $CaCO_3$ burial and a shallow CCD. The same scenario can be explained by changes in pelagic biogeochemical cycles. High production in one region results in a relatively large fraction of $CaCO_3$ surviving at the seafloor to be buried in the sediments. Whereas regions of both high and low $CaCO_3$ production will suffer from increased dissolution, the region of lower $CaCO_3$ production will be depleted of $CaCO_3$ first and, therefore, have a shallower CCD.

Changes in the total DIC content of the oceans can be driven by addition or removal of C_{org} or hydrocarbons as well as carbonate production. The most relevant example of this is the disappearance of $CaCO_3$ at the Paleocene/Eocene boundary, perhaps caused by a major release of methane trapped in gas hydrates (Dickens et al., 1995). The resulting increase in DIC drove down ocean pH and caused the CCD to shallow. In addition, high atmospheric CO_2 content is supported in this scenario. If organic matter is rapidly buried in shallow basins, the opposite effect can occur. Drawdown of the DIC pool with respect to alkalinity results in higher burial rates of $CaCO_3$ in the deep ocean and a deeper CCD, as well as lower atmospheric CO_2.

The indications of higher productivity associated with CAE-3 and CAE-4 imply that drawdown of DIC by organic burial in shallow basins may drive such events only if they are sufficiently decoupled from the pelagic nutrient cycles (i.e., lowering DIC does not lower total nutrient contents of the oceans as well). The shifts in CCD that we observe would not necessarily require huge changes in biogeochemical cycling (e.g., Broecker, 1982). Carbon is buried preferentially to the other nutrients, so burial of carbon in shallow sea basins or along continental margins may not require large losses of phosphorus or nitrogen. In addition, the storage of nutrients in the deep ocean buffers the effect of nutrient changes from productive regions. Changes in the rate of upwelling typically have a far larger effect on nutrient supply to the euphotic zone than changes in nutrient content.

The shelf-basin $CaCO_3$ fractionation scenario most intimately links changes in the CCD with glaciations. The slow buildup of the CAEs is consistent with a slow buildup of continental ice, but the shelf-basin fractionation cannot stop the continued development of glaciers. Another feedback mechanism must end the event. For CAE-3, the event ended by a transfer of DIC into the oceans as indicated by an abrupt shallowing of the CCD prior to an oxygen isotope change. Additional shallowing of the CCD followed, perhaps associated with the flooding of shelves and shallow seas or a movement of pelagic $CaCO_3$ depocenters away from equatorial regions. A decrease in productivity is associated with the $CaCO_3$ decline, but the decline of productivity itself was insufficient to cause the extreme shallowing of the CCD between CAE-3 and CAE-4.

CONCLUSIONS

We identified seven carbonate accumulation events in the middle and late Eocene and linked these events to global cooling. The events most probably mark periods of significant cooling in the high latitudes and may mark small glaciations that were reversed after 1–2 m.y. We have evidence that the largest of these events, CAE-3, was associated with elevated primary productivity and $CaCO_3$ production, but that $CaCO_3$ production was not necessarily highest at the Pacific equator. Instead, $CaCO_3$ production seems to be stronger south of the equatorial region. We observed changes in the carbon cycle independent of the productivity signal, signifying large changes in the ocean carbon reservoir. The repetition of the CAEs implies geosystem feedbacks that prevented large-scale development of ice sheets prior to the Eocene/Oligocene boundary, when the feedback mechanism apparently failed. Better delineation of the middle and late Eocene will improve our understanding of these events, but shelf-basin fractionation cannot be the only cause of increased $CaCO_3$ burial in the equatorial Pacific.

ACKNOWLEDGMENTS

We would like to thank all of the shipboard party of ODP Leg 199—ship's crew, drillers, technicians, and the scientific party—for their outstanding efforts to make the leg a success. Reviews by L. Peterson and W. Berger significantly improved the manuscript. This research used samples provided by the Ocean Drilling Program (ODP). ODP is sponsored by the U.S. National Science Foundation (NSF) and participating

countries under management of Joint Oceanographic Institutions (JOI), Inc. The study was funded by JOI/U.S. Science Advisory Committee (USSAC) and NSF grant OCE-0240906.

REFERENCES

Archer, D., Lyle, M., Rodgers, K., and Froelich, P., 1993. What controls opal preservation in tropical deep-sea sediments? *Paleoceanography,* 8:7–21.

Berger, W.H., Adelseck, C.G., and Mayer, L., 1976. Distribution of carbonate in surface sediments of the Pacific Ocean. *J. Geophys. Res.,* 81:2617–2627.

Berger, W.H., Vincent, E., and Thierstein, H.R., 1981. The deep-sea record: major steps in Cenozoic ocean evolution. *In* Warme, J.E., Douglas, R.G., and Winterer, E.L. (Eds.), *The Deep Sea Drilling Project: A Decade of Progress.* Spec. Publ.—Soc. Econ. Paleontol. Mineral., 32:489–504.

Bohaty, S., and Zachos, J., 2003. Significant Southern Ocean warming event in the late middle Eocene. *Geology,* 31(11):1017–1020.

Broecker, W.S., 1971. A kinetic model for the chemical composition of sea water. *Quat. Res.,* 1(2):188–207.

Broecker, W.S., 1982. Ocean chemistry during glacial time. *Geochim. Cosmochim. Acta,* 46:1689–1705.

Caldeira, K., and Wickett, M.E., 2003. Anthropogenic carbon and ocean pH. *Nature (London, U. K.),* 425:365.

Cande, S.C., and Kent, D.V., 1992. A new geomagnetic polarity time scale for the Late Cretaceous and Cenozoic. *J. Geophys. Res.,* 97:13917–13951.

Cande, S.C., and Kent, D.V., 1995. Revised calibration of the geomagnetic polarity timescale for the Late Cretaceous and Cenozoic. *J. Geophys. Res.,* 100:6093–6095.

Coxall, H.K., Wilson, P.A., Pälike, H., Lear, C.H., and Backman, J., 2005. Rapid stepwise onset of Antarctic glaciation and deeper calcite compensation in the Pacific Ocean. *Nature (London, U. K.),* 433(53–57):10.1038/nature03135.

Delaney, M.L., and Boyle, E.A., 1988. Tertiary paleoceanic chemical variability: unintended consequences of simple geochemical models. *Paleoceanography,* 3:137–156.

Demicco, R.V., Lowenstein, T.K., and Hardie, L.A., 2003. Atmospheric pCO_2 since 60 Ma from records of seawater pH, calcium, and primary carbonate mineralogy. *Geology,* 31(9):791–796.

Dickens, G.R., O'Neil, J.R., Rea, D.K., and Owen, R.M., 1995. Dissociation of oceanic methane hydrate as a cause of the carbon isotope excursion at the end of the Paleocene. *Paleoceanography,* 10:965–971.

Dickens, G.R., Castillo, M.M., and Walker, J.G.C., 1997. A blast of gas in the latest Paleocene: simulating first-order effects of massive dissociation of oceanic methane hydrate. *Geology,* 25:259–262.

Hardie, L.A., 1996. Secular variation in seawater chemistry: an explanation for the coupled secular variation in the mineralogies of marine limestones and potash evaporites of the past 600 m.y. *Geology,* 24(3):279–283.

Hartnett, H.E., and Devol, A.H., 2003. Role of a strong oxygen-deficient zone in the preservation and degradation matter: a carbon budget for the continental margins of northwest Mexico and Washington state. *Geochim. Cosmochim. Acta,* 67(2):247–264.

Honjo, S., Dymond, J., Collier, R., and Manganini, S.J., 1995. Export production of particles to the interior of the equatorial Pacific Ocean during the 1992 EqPac experiment. *Deep-Sea Res.,* 42:831–870.

Horita, J., Zimmermann, H., and Holland, H.D., 2002. Chemical evolution of seawater during the Phanerozoic: implications from the record of marine evaporites. *Geochem. Cosmochim. Acta,* 66(21):3733–3756.

Huber, M., and Caballero, R., 2003. Eocene El Nino: evidence for robust tropical dynamics in the "hothouse." *Science,* 299:877–881.

Karlin, G.M., Lyle, M., and Heath, G.R., 1987. Authigenic magnetite formation in suboxic marine sediments. *Nature (London, U. K.),* 326:490–493.

Lyle, M., Wilson, P.A., Janecek, T.R., et al., 2002. *Proc. ODP, Init. Repts.,* 199 [Online]. Available from World Wide Web: <http://www-odp.tamu.edu/publications/199_IR/199ir.htm>.

Lyle, M., 2003. Neogene carbonate burial in the Pacific Ocean. *Paleoceanography,* 18(3):10.1029/2002PA000777.

Miller, K.G., Wright, J.D., and Fairbanks, R.G., 1991. Unlocking the Ice House: Oligocene–Miocene oxygen isotopes, eustasy, and margin erosion. *J. Geophys. Res.,* 96:6829–6848.

Moore, T.C., Jr., Backman, J., Raffi, I., Nigrini, C., Sanfilippo, A., Pälike, H., and Lyle, M., 2004. Paleogene tropical Pacific: clues to circulation, productivity, and plate motion. *Paleoceanography,* 19:10.1029/2003PA000998.

Mortlock, R.A., and Froelich, P.N., 1989. A simple method for the rapid determination of biogenic opal in pelagic marine sediments. *Deep-Sea Res., Part A,* 36:1415–1426.

Murray, R.W., Leinen, M., and Isern, A.R., 1993. Biogenic flux of Al to sediment in the central equatorial Pacific Ocean: evidence for increased productivity during glacial periods. *Paleoceanography,* 8(5):651–670.

Musgrave, R.J., Delaney, M.L., Stax, R., and Tarduno, J.A., 1993. Magnetic diagenesis, organic input, interstitial water chemistry, and paleomagnetic record of the carbonate sequence on the Ontong Java Plateau. *In* Berger, W.H., Kroenke, L.W., Mayer, L.A., et al., *Proc. ODP, Sci. Results,* 130: College Station, TX (Ocean Drilling Program), 527–546.

Nelson, C.S., and Cooke, P.J., 2001. History of oceanic front development in the New Zealand sector of the Southern Ocean during the Cenozoic—a synthesis. *N. Z. J. Geol. Geophys.,* 44:535–553.

Olivarez Lyle, A., and Lyle, M.W., 2002. Determination of biogenic opal in pelagic marine sediments: a simple method revisited. *In* Lyle, M., Wilson, P.A., Janecek, T.R., et al., *Proc. ODP, Init. Repts.,* 199 [Online]. Available from World Wide Web: http://www-odp.tamu.edu/publications/199_IR/chap_06/chap_06.htm.

Pearson, P.N., and Palmer, M.R., 2000. Atmospheric carbon dioxide concentrations over the past 60 million years. *Nature (London, U.K.),* 406:695–699.

Peterson, L.C., Murray, D.W., Ehrmann, W.U., and Hempel, P., 1992. Cenozoic carbonate accumulation and compensation depth changes in the Indian Ocean. *In* Duncan, R.A., Rea, D.K., Kidd, R.B., von Rad, U., and Weissel, J.K. (Eds.), *Synthesis of Results from Scientific Drilling in the Indian Ocean.* Geophys. Monogr., 70:311–333.

Pisias, N.G., Mayer, L.A., and Mix, A.C., 1995. Paleoceanography of the eastern equatorial Pacific during the Neogene: synthesis of Leg 138 drilling results. *In* Pisias, N.G., Mayer, L.A., Janecek, T.R., Palmer-Julson, A., and van Andel, T.H. (Eds.), *Proc. ODP, Sci. Results,* 138: College Station, TX (Ocean Drilling Program), 5–21.

Rea, D.K., and Lyle, M.W., 2005. Paleogene calcite compensation depth in the eastern subtropical Pacific: answers and questions. *Paleoceanography,* 20(1):10.1029/2004PA001064.

Royer, D.L., Berner, R.A., Montaez, I.P., Tabor, N.J., and Beerling, D.J., 2004. CO_2 as a primary driver of Phanerozoic climate. *GSA Today,* 14(3):4–10.

Shellito, C.J., Sloan, L.C., and Huber, M., 2003. Climate model sensitivity to atmospheric CO_2 levels in the early–middle Paleogene. *Palaeogeogr., Palaecoclimatol., Palaeoecol.,* 193:113–123.

Tarduno, J.A, Duncan, R.A., Scholl, D.W., Cottrell, R.D., Steinberger, B., Thordarson, T., Kerr, B.C., Neal, C.R., Frey, F.A., Torii, M., and Carvallo, C., 2003. The Emperor Seamounts: southward motion of the Hawaiian hotspot plume in Earth's mantle. *Science,* 301(22):1064–1069.

Thomas, D.J., Zachos, J.C., Bralower, T.J., Thomas, E., and Bohaty, S., 2002. Warming the fuel for the fire: evidence for the thermal dissociation of methane hydrate during the Paleocene–Eocene Thermal Maximum. *Geology,* 30(12):1067–1070.

Tripati, A., Backman, J., Elderfield, H., and Ferreti, P., 2005, Eocene bipolar glaciation associated with global carbon cycle changes. *Nature,* 436:341-345.

van Andel, T.H., Heath, G.R., et al., 1973. *Init. Repts. DSDP,* 16: Washington (U.S. Govt. Printing Office).

van Andel, T.H., 1975. Mesozoic/Cenozoic calcite compensation depth and the global distribution of calcareous sediments. *Earth Planet. Sci. Lett.,* 26:187–194.

Veizer, J., Godderis, Y., and Francois, L.M., 2000. Evidence for decoupling of atmospheric CO_2 and global climate during the Phanerozoic eon. *Nature (London, U. K.),* 408:698–701.

Zachos, J., Pagani, M., Sloan, L., Thomas, E., and Billups, K., 2001. Trends, rhythms, and aberrations in global climate 65 Ma to present. *Science,* 292:686–693.

APPENDIX

Absolute Pole Rotations

Age (Ma)	Pacific plate/ Hotspot Euler Pole °N	°E	Rotation (°/m.y.)	Latitude (°)	Longitude (°)	Colatitude distance from great circle (km)	Earth radius at colatitude (km)	Bearing of rotation pole from north (°)	Bearing of backtrack* (°)	Δ Latitude	Δ Longitude	Movement (km/m.y.)
Site 1215												
0	60.20	–90.00	0.980	26.03	–147.93	51.839	5009.38	32.39	122.39	–0.413	0.725	85.682
1	60.20	–90.00	0.980	25.61	–147.21	51.840	5009.47	32.10	122.10	–0.410	0.725	85.683
2	60.20	–90.00	0.980	25.20	–146.48	51.842	5009.57	31.80	121.80	–0.407	0.725	85.685
3	60.20	–90.00	0.980	24.80	–145.76	51.843	5009.67	31.50	121.50	–0.403	0.725	85.687
4	60.20	–90.00	0.980	24.39	–145.03	51.845	5009.77	31.19	121.19	–0.400	0.725	85.688
5	60.20	–90.00	0.980	23.99	–144.31	51.846	5009.88	30.88	120.88	–0.396	0.725	85.690
6	69.00	–71.00	0.791	23.60	–143.58	61.834	5616.54	22.82	112.82	–0.271	0.703	77.540
7	69.00	–71.00	0.791	23.33	–142.88	61.834	5616.56	22.73	112.73	–0.270	0.702	77.540
8	69.00	–71.00	0.791	23.06	–142.18	61.834	5616.58	22.63	112.63	–0.269	0.701	77.540
9	69.00	–71.00	0.791	22.79	–141.48	61.835	5616.60	22.53	112.53	–0.268	0.700	77.540
10	69.00	–71.00	0.791	22.52	–140.78	61.835	5616.62	22.42	112.42	–0.266	0.699	77.541
11	69.00	–71.00	0.791	22.25	–140.08	61.835	5616.64	22.32	112.32	–0.265	0.698	77.541
12	69.00	–71.00	0.791	21.99	–139.38	61.836	5616.66	22.20	112.20	–0.264	0.698	77.541
13	69.00	–71.00	0.791	21.73	–138.68	61.836	5616.69	22.09	112.09	–0.263	0.697	77.542
14	69.00	–71.00	0.791	21.46	–137.99	61.837	5616.72	21.97	111.97	–0.261	0.696	77.542
15	69.00	–71.00	0.791	21.20	–137.29	61.837	5616.74	21.85	111.85	–0.260	0.695	77.542
16	69.00	–71.00	0.791	20.94	–136.59	61.838	5616.77	21.73	111.73	–0.259	0.695	77.543
17	69.00	–71.00	0.791	20.68	–135.90	61.838	5616.80	21.60	111.60	–0.257	0.694	77.543
18	69.00	–71.00	0.791	20.43	–135.20	61.839	5616.83	21.47	111.47	–0.256	0.694	77.543
19	69.00	–71.00	0.791	20.17	–134.51	61.840	5616.86	21.33	111.33	–0.254	0.693	77.544
20	69.00	–71.00	0.791	19.92	–133.82	61.840	5616.90	21.20	111.20	–0.253	0.693	77.544
21	69.00	–71.00	0.791	19.66	–133.13	61.841	5616.93	21.06	111.06	–0.251	0.692	77.545
22	69.00	–71.00	0.791	19.41	–132.43	61.842	5616.97	20.92	110.92	–0.249	0.692	77.545
23	69.00	–71.00	0.791	19.16	–131.74	61.842	5617.01	20.77	110.77	–0.248	0.692	77.546
24	69.00	–71.00	0.791	18.92	–131.05	61.843	5617.04	20.62	110.62	–0.246	0.691	77.546
25	69.00	–71.00	0.791	18.67	–130.36	61.844	5617.08	20.47	110.47	–0.244	0.691	77.547
26	69.00	–71.00	0.791	18.42	–129.67	61.845	5617.12	20.32	110.32	–0.243	0.691	77.548
27	69.00	–71.00	0.791	18.18	–128.98	61.845	5617.17	20.16	110.16	–0.241	0.690	77.548
28	69.00	–71.00	0.791	17.94	–128.29	61.846	5617.21	20.00	110.00	–0.239	0.690	77.549
29	69.00	–71.00	0.693	17.70	–127.60	61.847	5617.25	19.84	109.84	–0.208	0.604	67.941
30	69.00	–71.00	0.693	17.49	–126.99	61.848	5617.29	19.69	109.69	–0.206	0.604	67.942
31	69.00	–71.00	0.693	17.29	–126.39	61.848	5617.32	19.54	109.54	–0.205	0.604	67.942
32	69.00	–71.00	0.693	17.08	–125.78	61.849	5617.36	19.39	109.39	–0.203	0.604	67.943
33	69.00	–71.00	0.693	16.88	–125.18	61.850	5617.40	19.24	109.24	–0.202	0.604	67.943
34	69.00	–71.00	0.693	16.68	–124.58	61.850	5617.43	19.09	109.09	–0.200	0.604	67.944
35	69.00	–71.00	0.693	16.48	–123.97	61.851	5617.47	18.93	108.93	–0.199	0.604	67.944
36	69.00	–71.00	0.693	16.28	–123.37	61.852	5617.51	18.78	108.78	–0.197	0.604	67.945
37	69.00	–71.00	0.693	16.08	–122.76	61.853	5617.55	18.62	108.62	–0.195	0.604	67.945
38	69.00	–71.00	0.693	15.89	–122.16	61.853	5617.59	18.46	108.46	–0.194	0.604	67.946
39	69.00	–71.00	0.693	15.69	–121.56	61.854	5617.63	18.29	108.29	–0.192	0.604	67.946
40	69.00	–71.00	0.693	15.50	–120.95	61.855	5617.67	18.13	108.13	–0.190	0.604	67.947
41	69.00	–71.00	0.693	15.31	–120.35	61.856	5617.72	17.96	107.96	–0.189	0.604	67.947
42	69.00	–71.00	0.693	15.12	–119.75	61.857	5617.76	17.79	107.79	–0.187	0.604	67.948
43	69.00	–71.00	0.693	14.94	–119.14	61.857	5617.80	17.62	107.62	–0.185	0.604	67.948
44	22.00	–91.00	0.652	14.75	–118.54	27.074	2899.70	70.36	160.36	–0.280	0.103	32.997
45	22.00	–91.00	0.652	14.47	–118.43	27.075	2899.83	69.81	159.81	–0.279	0.106	32.999
46	22.00	–91.00	0.652	14.19	–118.33	27.077	2899.97	69.25	159.25	–0.278	0.109	33.000
47	22.00	–91.00	0.652	13.91	–118.22	27.078	2900.11	68.70	158.70	–0.277	0.111	33.002
48	22.00	–91.00	0.652	13.64	–118.11	27.079	2900.24	68.14	158.14	–0.276	0.114	33.003
49	22.00	–91.00	0.652	13.36	–118.00	27.081	2900.38	67.59	157.59	–0.275	0.117	33.005
50	22.00	–91.00	0.652	13.09	–117.88	27.082	2900.52	67.03	157.03	–0.274	0.119	33.007
51	22.00	–91.00	0.652	12.81	–117.76	27.084	2900.65	66.48	156.48	–0.273	0.122	33.008
52	22.00	–91.00	0.652	12.54	–117.64	27.085	2900.79	65.92	155.92	–0.272	0.124	33.010
53	22.00	–91.00	0.652	12.27	–117.51	27.086	2900.93	65.37	155.37	–0.270	0.127	33.011
54	22.00	–91.00	0.652	12.00	–117.39	27.088	2901.07	64.81	154.81	–0.269	0.129	33.013
55	22.00	–91.00	0.652	11.73	–117.26	27.089	2901.20	64.26	154.26	–0.268	0.132	33.014
56	22.00	–91.00	0.652	11.46	–117.13	27.091	2901.34	63.70	153.70	–0.267	0.134	33.016
57	22.00	–91.00	0.652	11.19	–116.99	27.092	2901.48	63.15	153.15	–0.265	0.137	33.017
58	22.00	–91.00	0.652	10.93	–116.85	27.093	2901.61	62.59	152.59	–0.264	0.139	33.019

Notes: Absolute pole rotations from Engebretson et al. (1985; table 2), and Gripp and Gordon (1990). Calculations are for 0- to 5-Ma rotation. Earth's radius = 6371 km. Only a portion of this table appears here. The complete table is available in **ASCII**.

Figure F1. Site map showing locations of Sites 1218, 1219, and 1220. F.Z. = fracture zone (from Lyle, Wilson, Janecek, et al., 2002).

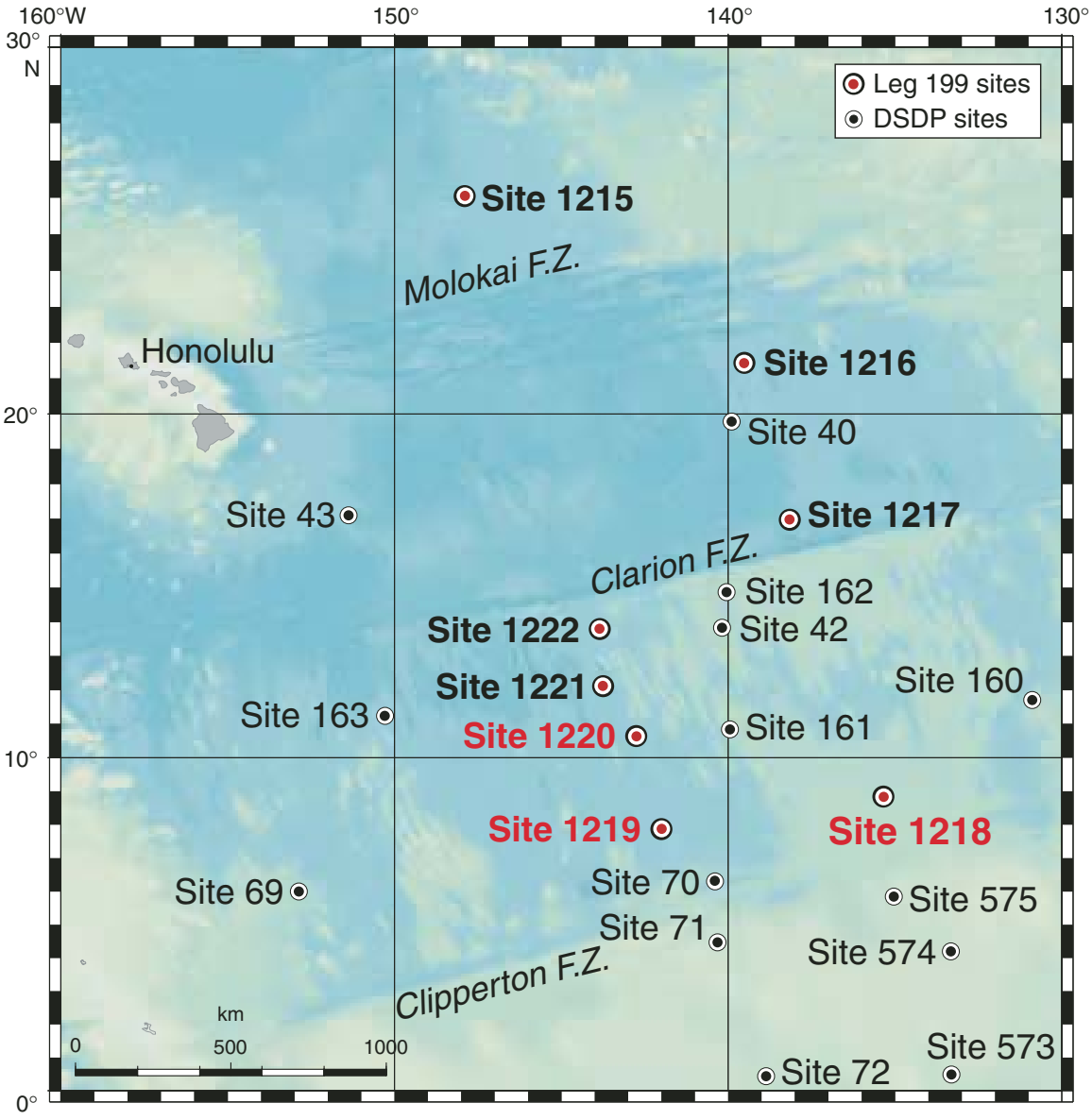

Figure F2. Time series for $CaCO_3$, biogenic SiO_2 on a carbonate-free basis, and carbonate-free C_{org}. Carbonate accumulation events (CAEs) occur every 1–2 m.y., but a large response in the other biogenic sediment fractions occurs only between 41.5 and 38.2 Ma.

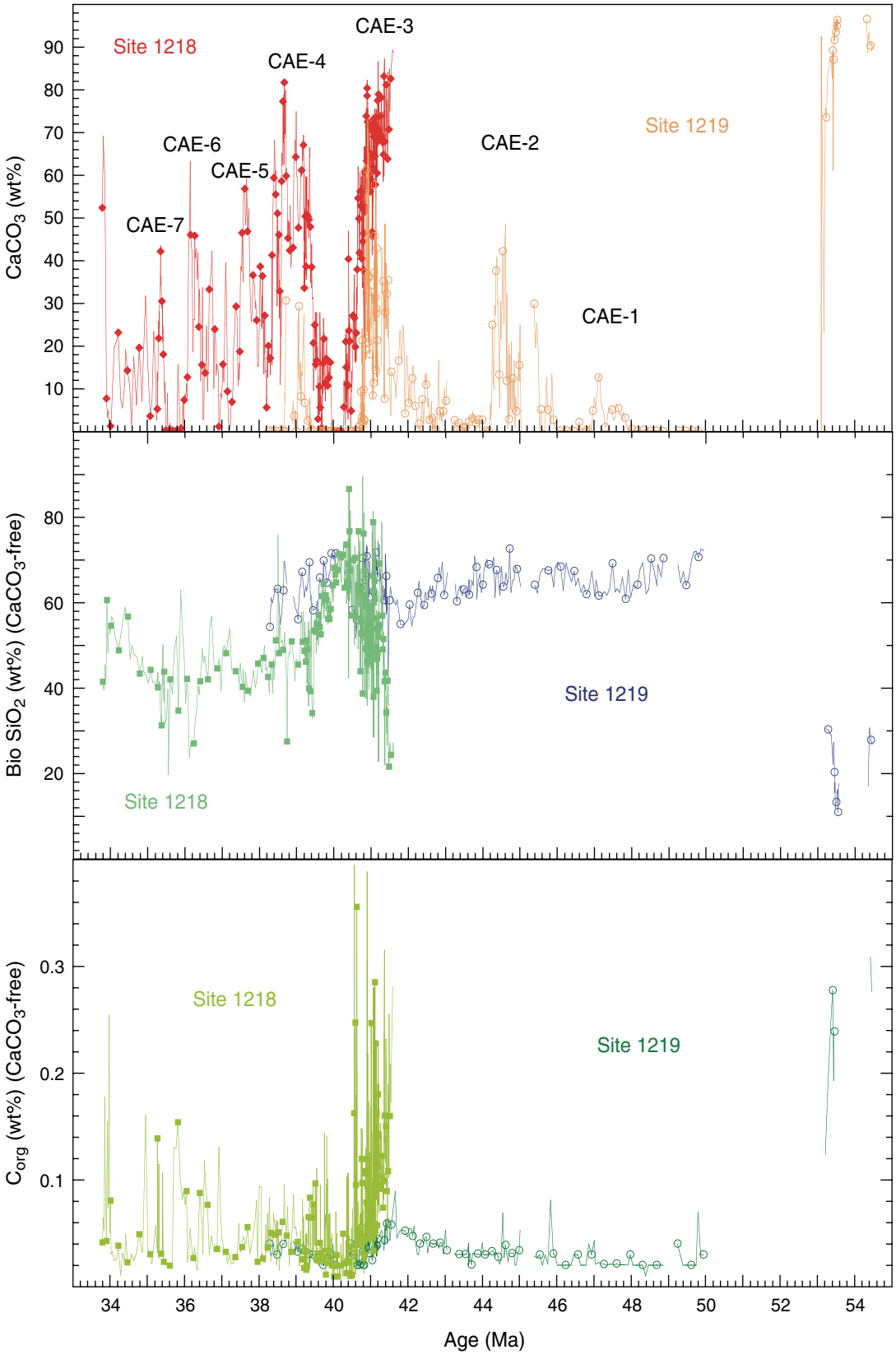

Figure F3. Time series for $CaCO_3$ mass accumulation rate (MAR), biogenic SiO_2 MAR, and C_{org} MAR. MAR time series better show that the carbonate accumulation events (CAEs) between 41.5 and 38.2 Ma are much larger than the other Eocene events.

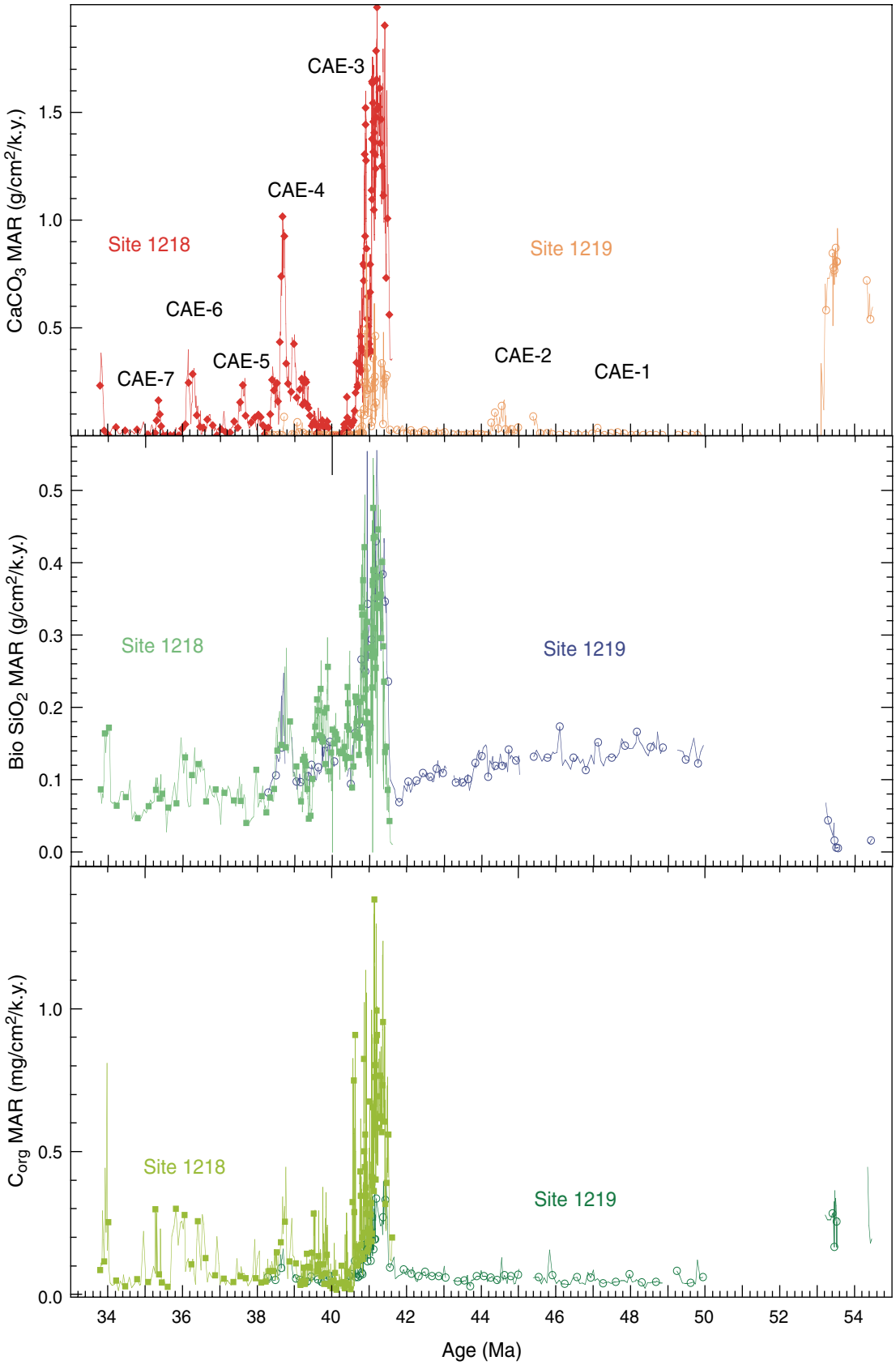

Figure F4. Detail of interval from 43 to 37 Ma from (**A**) Site 1218 and (**B**) Site 1219 to show that $CaCO_3$ mass accumulation rate (MAR) disappears while biogenic SiO_2 MAR remains relatively high. The exaggerated decrease in $CaCO_3$ MAR indicates much stronger dissolution in the interval between 40.7 and 39.6 Ma.

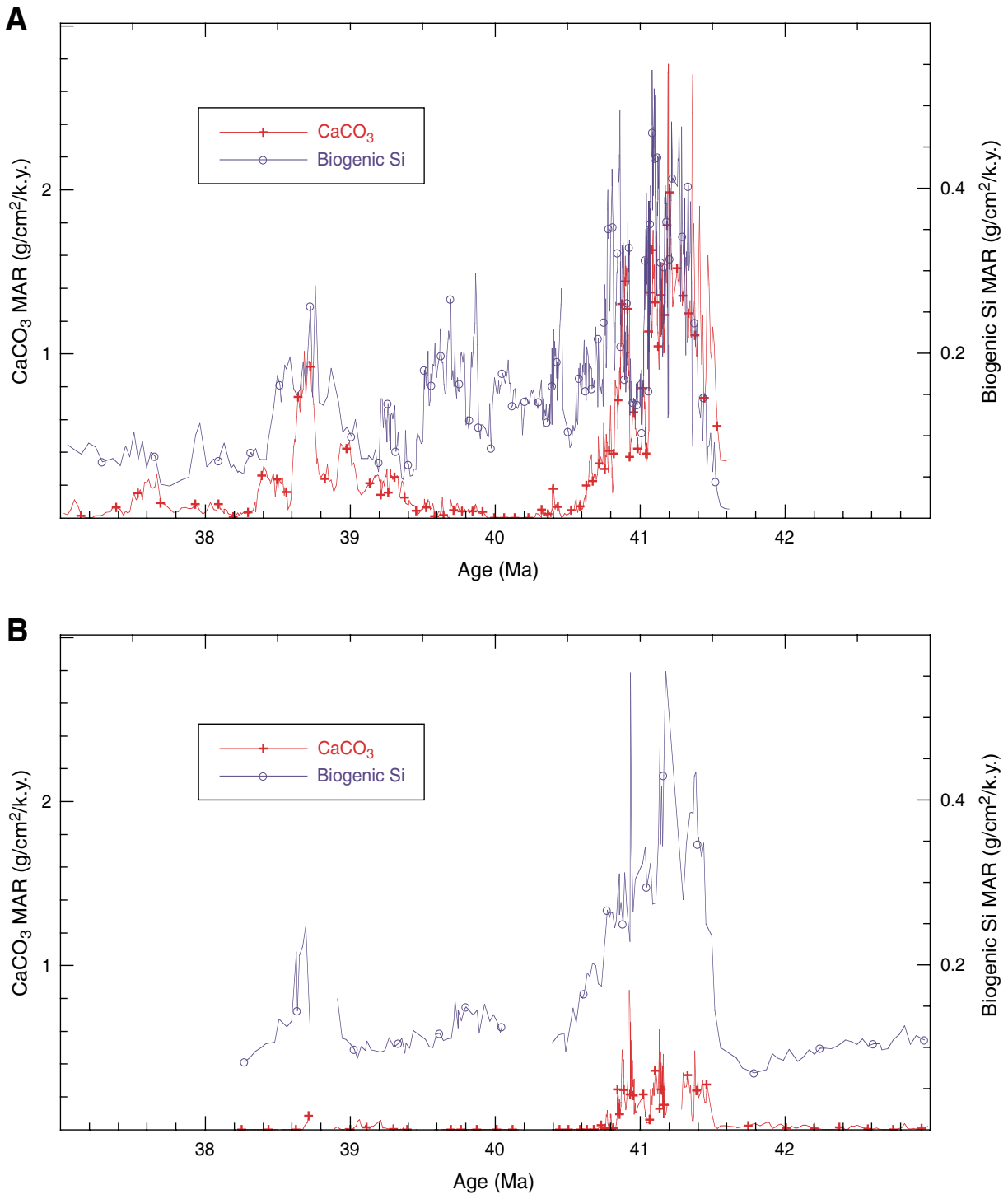

Figure F5. An example of CCD change estimated using percentages vs. $CaCO_3$ mass accumulation rate (MAR) using two sites. Because the change in carbonate weight percent is not equivalent to the mass of $CaCO_3$ dissolved except when $CaCO_3$ is below 50 wt%, the use of percentage data tends to significantly overestimate the depth to the CCD. Changes in MAR between two sites with different depths but the same $CaCO_3$ rain will give the correct CCD.

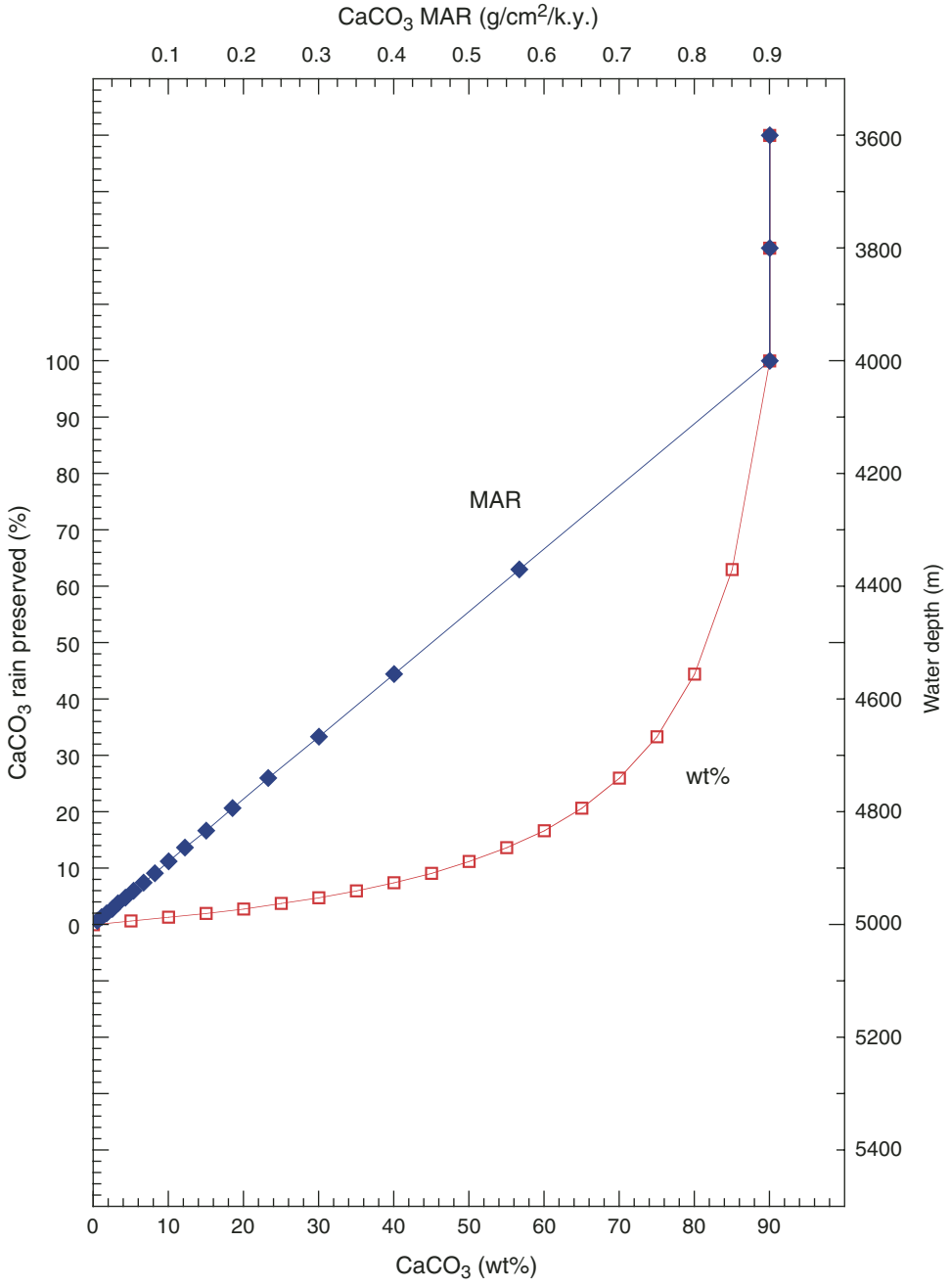

Figure F6. CCD estimate based on Sites 1218, 1219, and 1220 over CAE-3. Sites 1218 and 1220 were at the equator at 40 Ma, while Site 1219 was at ~2°S. The lack of $CaCO_3$ at Site 1220 is in contradiction with the large changes that occur at both Sites 1218 and 1219. The Site 1220 data indicate either sediment bypassing at Site 1220 or somewhat higher $CaCO_3$ production away from the equator. MAR = mass accumulation rate.

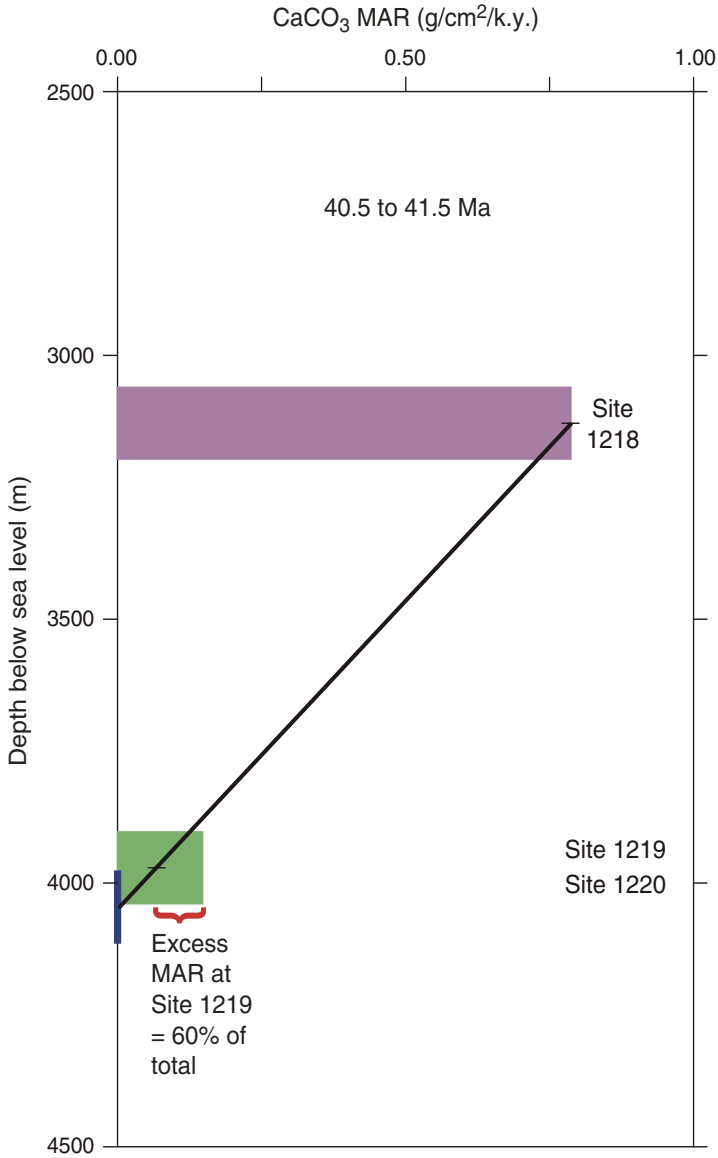

Figure F7. Bulk oxygen isotopes at Site 1219 and $CaCO_3$. We observe a general correlation of high oxygen isotopes with high $CaCO_3$. For carbonate accumulation event (CAE)-2 (45.9–44.2 Ma) and CAE-3 (42.2–40.5 Ma), especially, we observe high $CaCO_3$ correlates with high oxygen isotopes. The CAE intervals coincide with cool conditions and/or polar ice. PDB = Peedee belemnite.

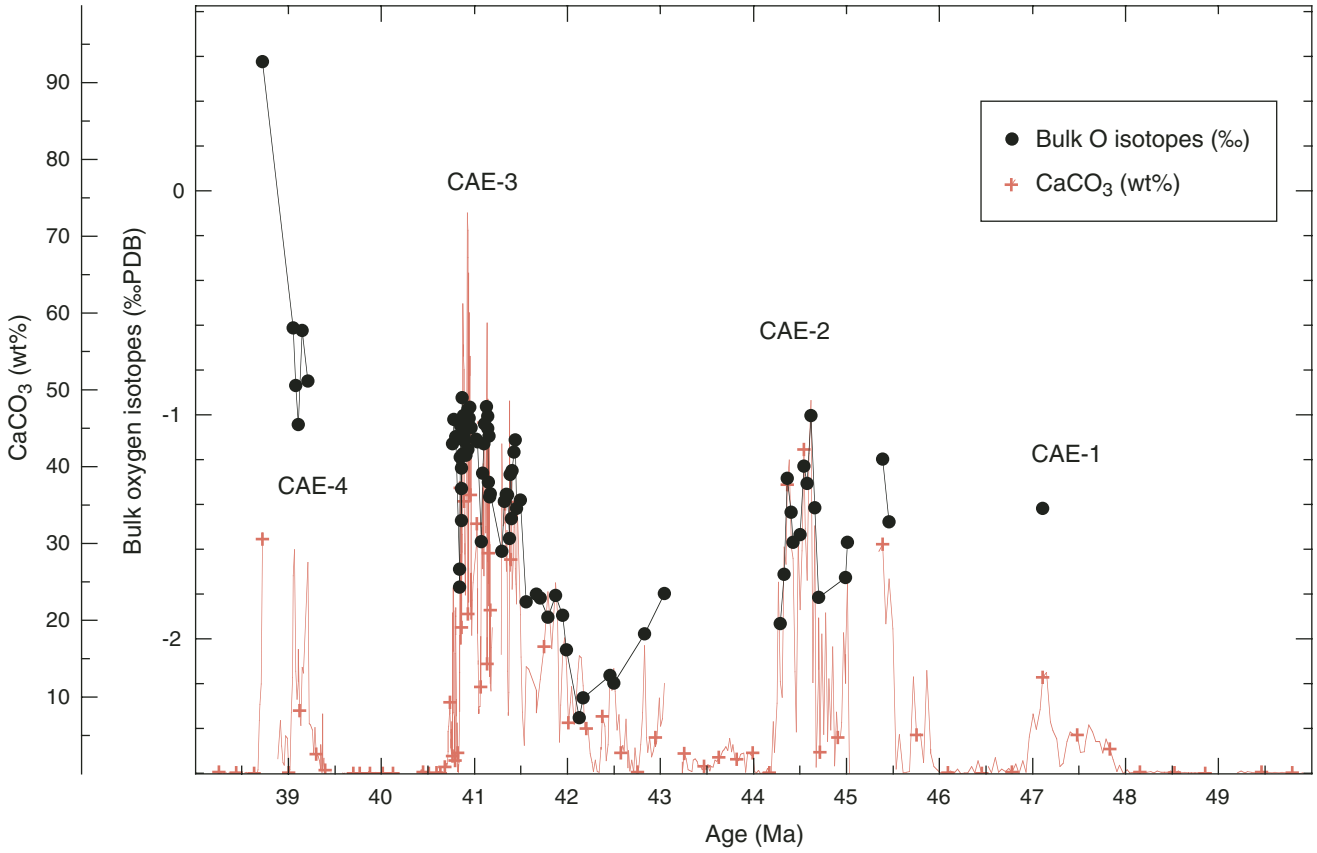

Figure F8. (A) Oxygen isotope and (B) carbon isotope records from the benthic foraminifer *Nutalloides trumpeyii*. The records show, along with bulk oxygen isotope records (Fig. F7, p. 28), that the end of carbonate accumulation event (CAE)-3 occurred prior to any warming and was associated with an extremely large $\delta^{13}C$ event in deep water. PDB = Peedee belemnite. MAR = mass accumulation rate.

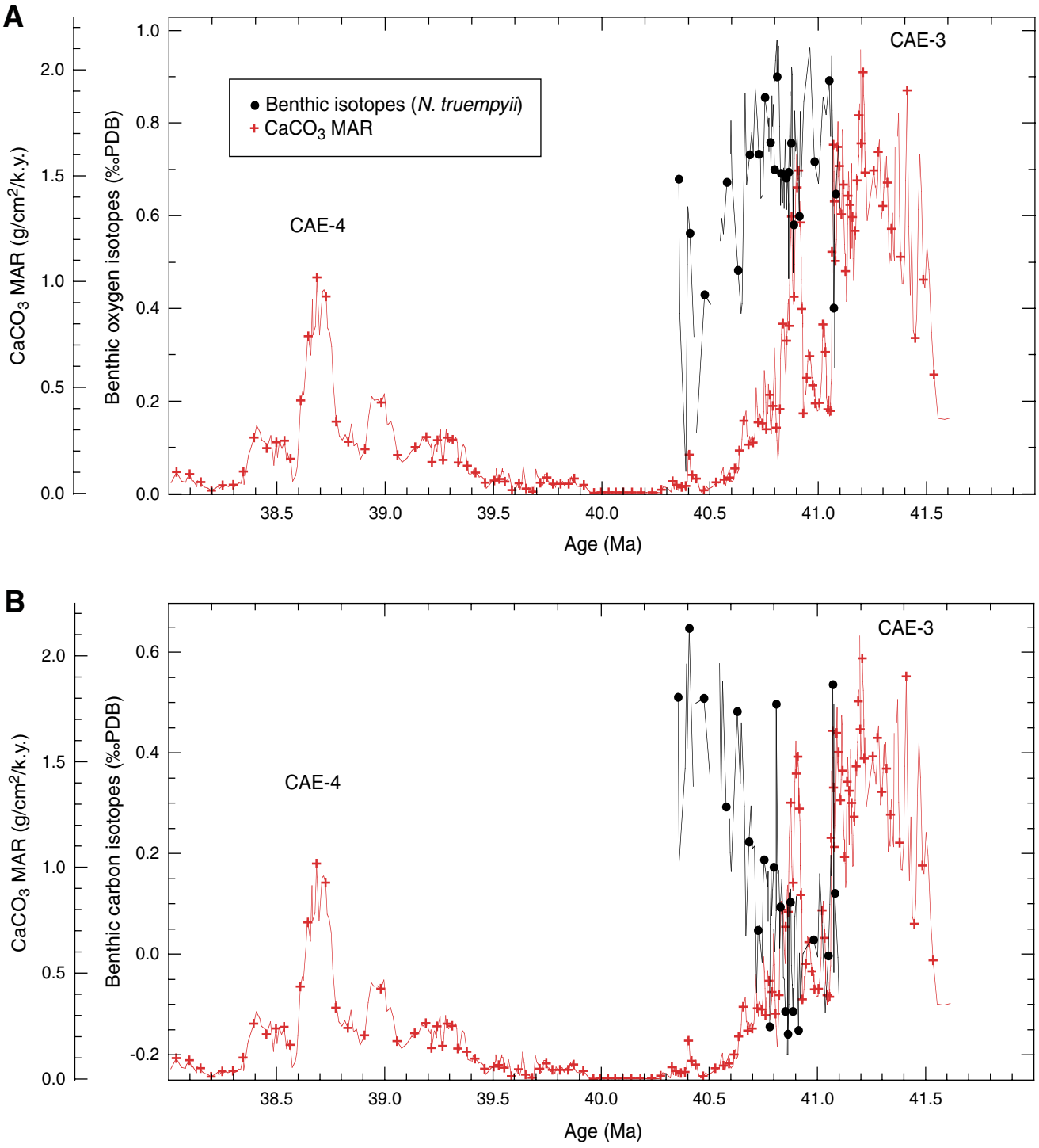

Table T1. C_{org}, $CaCO_3$, and opal, Site 1218.

Core, section, interval (cm)	Offset (m)	Average depth (mbsf)	Average depth (mcd)	Average depth (rmcd)*	1218 rmcd equivalent depth (m)	Age† (Ma)	Paleo-latitude (°N)	Paleo-longitude (°E)	Bulk density (g/cm³) Wet	Bulk density (g/cm³) Dry	LSR (m/m.y.)	Total MAR (g/cm²/k.y.)	C_{org} Content (wt%)	C_{org} MAR (mg/cm²/k.y.)	$CaCO_3$ Content (wt%)	$CaCO_3$ MAR (g/cm²/k.y.)	Biogenic SiO_2 Content (wt%)	Biogenic SiO_2 MAR (g/cm²/k.y.)	$CaCO_3$ data source
199-1218A-																			
26X-1, 10–11	26.07	234.405	260.475	261.026	261.026	38.06	0.32	–108	1.293	0.510	4.217	0.215	0.02	0.04	24.7	0.05	33.1	0.07	BSU
26X-1, 30–31	26.07	234.605	260.675	261.168	261.168	38.094	0.31	–107.98	1.323	0.553	4.252	0.235	0.02	0.05	36.4	0.09	29.7	0.07	BSU
26X-1, 50–51	26.07	234.805	260.875	261.31	261.31	38.128	0.31	–107.95	1.282	0.493	4.286	0.211	0.02	0.04	13.5	0.03	43.2	0.09	BSU
26X-1, 70–71	26.07	235.005	261.075	261.452	261.452	38.163	0.3	–107.93	1.238	0.429	4.255	0.183	0.02	0.04	14.2	0.03	38.0	0.07	BSU
26X-1, 90–91	26.07	235.205	261.275	261.594	261.594	38.196	0.3	–107.91	1.190	0.358	4.289	0.154	0.03	0.05	5.7	0.01	41.9	0.06	BSU
26X-1, 110–111	26.07	235.405	261.475	261.736	261.736	38.23	0.29	–107.89	1.188	0.355	4.322	0.153	0.06	0.09	12.8	0.02	37.2	0.06	BSU
26X-1, 130–131	26.07	235.605	261.675	261.878	261.878	38.263	0.29	–107.87	1.219	0.400	4.355	0.174	0.03	0.05	20.9	0.04	30.7	0.05	BSU
26X-2, 10–11	26.07	235.905	261.975	262.091	262.091	38.313	0.28	–107.83	1.272	0.479	4.406	0.211	0.02	0.04	16.6	0.04	37.9	0.08	BSU
26X-2, 30–31	26.07	236.105	262.175	262.233	262.233	38.346	0.28	–107.81	1.340	0.578	4.439	0.257	0.04	0.10	15.6	0.04	32.8	0.08	BSU
26X-2, 50–51	26.07	236.305	262.375	262.375	262.375	38.38	0.27	–107.79	1.538	0.870	4.472	0.389	0.03	0.12	56.7	0.22	18.2	0.07	BSU
26X-2, 70–71	26.07	236.505	262.575	262.575	262.575	38.427	0.26	–107.76	1.581	0.933	4.519	0.422	0.02	0.08	59.2	0.25	20.9	0.09	BSU
26X-2, 90–91	26.07	236.705	262.775	262.775	262.775	38.469	0.26	–107.73	1.434	0.716	7.341	0.526	0.03	0.16	51.4	0.27	24.6	0.13	BSU
26X-2, 110–111	26.07	236.905	262.975	262.975	262.975	38.495	0.25	–107.72	1.341	0.580	8.019	0.465	0.03	0.14	51.1	0.24	37.2	0.17	BSU
26X-2, 130–131	26.07	237.105	263.175	263.175	263.175	38.52	0.25	–107.7	1.371	0.623	8.044	0.501	0.03	0.15	41.6	0.21	28.2	0.14	BSU
26X-3, 10–11	26.07	237.405	263.475	263.475	263.475	38.558	0.24	–107.68	1.352	0.596	8.081	0.482	0.02	0.10	29.3	0.14	37.6	0.18	BSU
26X-3, 30–31	26.07	237.605	263.675	263.675	263.675	38.583	0.24	–107.66	1.338	0.576	8.106	0.467	0.03	0.14	17.5	0.08	41.8	0.19	BSU
26X-3, 50–51	26.07	237.805	263.875	263.875	263.875	38.608	0.24	–107.64	1.566	0.911	8.131	0.741	0.02	0.15	58.6	0.43	21.2	0.16	BSU
26X-3, 70–71	26.07	238.005	264.075	264.075	264.075	38.632	0.23	–107.63	1.606	0.970	9.565	0.928	0.02	0.19	67.2	0.62	16.1	0.15	BSU
26X-3, 90–91	26.07	238.205	264.275	264.275	264.275	38.653	0.23	–107.61	1.628	1.002	9.586	0.961	0.02	0.19	67.6	0.65	16.2	0.16	BSU
26X-3, 110–111	26.07	238.405	264.475	264.475	264.475	38.674	0.23	–107.6	1.756	1.190	9.607	1.143	0.03	0.34	68.8	0.79	16.6	0.19	BSU
26X-3, 130–131	26.07	238.605	264.675	264.675	264.675	38.694	0.22	–107.59	1.701	1.109	9.628	1.068	0.02	0.21	69.7	0.74	15.1	0.16	BSU
26X-4, 10–11	26.07	238.905	264.975	264.975	264.975	38.724	0.22	–107.57	1.809	1.268	12.201	1.547	0.02	0.31	59.8	0.93	16.6	0.26	BSU
26X-4, 30–31	26.07	239.105	265.175	265.175	265.175	38.741	0.22	–107.56	1.663	1.053	12.218	1.287	0.02	0.26	58.7	0.76	11.4	0.15	BSU
26X-4, 50–51	26.07	239.305	265.375	265.375	265.375	38.757	0.22	–107.55	1.567	0.913	12.234	1.117	0.04	0.45	46.5	0.52	25.2	0.28	BSU
26X-4, 70–71	26.07	239.505	265.575	265.575	265.575	38.784	0.21	–107.53	1.483	0.788	7.130	0.562	0.02	0.11	48.0	0.27	25.0	0.14	BSU
26X-4, 90–91	26.07	239.705	265.775	265.775	265.775	38.812	0.21	–107.51	1.477	0.780	7.158	0.558	0.01	0.06	49.0	0.27	24.6	0.14	BSU
26X-4, 110–111	26.07	239.905	265.975	265.975	265.975	38.84	0.2	–107.49	1.498	0.811	7.572	0.614	0.02	0.12	53.0	0.33	24.1	0.15	BSU
26X-4, 130–131	26.07	240.105	266.175	266.175	266.175	38.866	0.2	–107.48	1.474	0.775	7.599	0.589	0.02	0.12	39.7	0.23	30.8	0.18	BSU
26X-5, 10–11	26.07	240.405	266.475	266.475	266.475	38.92	0.19	–107.44	1.561	0.903	7.379	0.666	0.04	0.27	53.8	0.36	21.2	0.14	BSU
26X-5, 30–31	26.07	240.605	266.675	266.675	266.675	38.947	0.19	–107.42	1.579	0.929	7.406	0.688	0.02	0.14	63.5	0.44	15.2	0.10	BSU
26X-5, 50–51	26.07	240.805	266.875	266.875	266.875	38.978	0.18	–107.4	1.628	1.001	6.605	0.661	0.02	0.13	64.3	0.43	16.7	0.11	BSU
26X-5, 70–71	26.07	241.005	267.075	267.075	267.075	39.008	0.18	–107.38	1.494	0.805	6.635	0.534	0.02	0.11	59.9	0.32	18.6	0.10	BSU
26X-5, 90–91	26.07	241.205	267.275	267.275	267.275	39.036	0.17	–107.37	1.431	0.713	7.793	0.556	0.02	0.11	52.9	0.29	21.5	0.12	BSU
26X-5, 110–111	26.07	241.405	267.475	267.475	267.475	39.075	0.17	–107.34	1.425	0.703	4.249	0.299	0.01	0.03	47.8	0.14	24.1	0.07	BSU
26X-5, 130–131	26.07	241.605	267.675	267.675	267.675	39.122	0.16	–107.31	1.463	0.760	4.296	0.326	0.02	0.07	61.8	0.20	22.1	0.07	BSU
26X-6, 11–12	26.07	241.915	267.985	267.983	267.983	39.195	0.15	–107.26	1.528	0.855	4.369	0.374	0.02	0.07	69.4	0.26	15.0	0.06	BSU
26X-6, 30–31	26.07	242.105	268.175	268.16	268.16	39.225	0.15	–107.24	1.396	0.661	6.924	0.458	0.02	0.09	48.3	0.22	26.6	0.12	BSU
26X-6, 50–51	26.07	242.305	268.375	268.348	268.348	39.252	0.14	–107.23	1.434	0.717	6.951	0.498	0.02	0.10	59.8	0.30	18.5	0.09	BSU
26X-6, 70–71	26.07	242.505	268.575	268.536	268.536	39.279	0.14	–107.21	1.435	0.718	6.978	0.501	0.02	0.10	59.5	0.30	16.6	0.08	BSU
26X-6, 90–91	26.07	242.705	268.775	268.723	268.723	39.306	0.13	–107.19	1.426	0.705	7.005	0.494	0.02	0.10	48.8	0.24	26.8	0.13	BSU
26X-6, 110–111	26.07	242.905	268.975	268.911	268.911	39.335	0.13	–107.17	1.427	0.707	4.071	0.288	0.01	0.03	49.6	0.14	27.0	0.08	BSU
26X-6, 130–131	26.07	243.105	269.175	269.099	269.099	39.381	0.12	–107.14	1.383	0.641	4.117	0.264	0.02	0.05	34.9	0.09	40.2	0.11	BSU

Notes: * = **Pälike et al.,** this volume. † = H. Pälike, unpubl. data, LSR = linear sedimentation rate, MAR = mass accumulation rate, BSU = Boise State University. Only a portion of this table appears here. The complete version of this table is available in **ASCII.**

Table T2. C_{org}, $CaCO_3$, biogenic opal, and bulk $\delta^{18}O$ and $\delta^{13}C$ data, Hole 1219A.

Core, section, interval (cm)	Average depth (mbsf)	Average depth (mcd)	Average depth (rmcd)	1218 rmcd equivalent depth (m)	Age (Ma)	Paleo-latitude (°N)	Paleo-longitude (°E)	Bulk density (g/cm³) Wet	Bulk density (g/cm³) Dry	LSR (m/m.y.)	Total MAR (g/cm²/k.y.)	C_{org} (wt%)	$CaCO_3$ (wt%)	Biogenic SiO_2 (wt%)	Analytical facility	ID	$\delta^{13}C$ (‰ PDB)	$\delta^{18}O$ (‰ PDB)	Standard deviation 45/44	Standard deviation 46/44	Analytical facility
199-1219A-																					
13H-3, 50–54	113.58	133.17	130.33	190.67	29.720	–0.10	–119.80	1.68	1.053	15.823	1.666	0.03	87.17	4.9	BSU						
16H-6, 50–54	147.13	171.46	168.62	232.64	33.042	–0.72	–117.65	1.63	0.973	10.716	1.043	0.01	73.4	10.9	BSU						
17H-6, 50–54	155.39	180.72	177.88	244.76	34.371	–0.96	–116.78	1.19	0.316	4.669	0.148	0.02	1.49	52.3	BSU						
19H-5, 0–1	173.505	200.835	198.00	261.86	38.252	–1.64	–114.25			4.635			0.18		Stockholm						
19H-5, 10–11	173.605	200.935	198.09	261.94	38.270	–1.64	–114.24	1.20	0.326	4.652	0.152	0.04	0.08	54.2	BSU						
19H-5, 20–21	173.705	201.035	198.20	262.03	38.290	–1.64	–114.23	1.20	0.342	4.672	0.160		0.18		Stockholm						
19H-5, 30–31	173.805	201.135	198.29	262.11	38.308	–1.65	–114.22	1.18	0.308	4.690	0.144	0.03	0.06	61.1	BSU						
19H-5, 40–41	173.905	201.235	198.39	262.19	38.325	–1.65	–114.21	1.20	0.342	4.707	0.161		0.16		Stockholm						
19H-5, 50–51	174.005	201.335	198.50	262.28	38.345	–1.65	–114.19	1.20	0.337	4.727	0.159	0.03	0.07	59.9	BSU						
19H-5, 60–61	174.105	201.435	198.59	262.36	38.363	–1.66	–114.18			4.745			0.16		Stockholm						
19H-5, 70–71	174.205	201.535	198.70	262.45	38.382	–1.66	–114.17			4.765		0.04	0.05	61.6	BSU						
19H-5, 80–81	174.305	201.635	198.79	262.52	38.398	–1.66	–114.16			4.780			0.13		Stockholm						
19H-5, 90–91	174.405	201.735	198.89	262.61	38.418	–1.67	–114.15	1.20	0.343	4.800	0.165	0.03	0.08	63.1	BSU						
19H-5, 100–101	174.505	201.835	199.00	262.70	38.437	–1.67	–114.13	1.20	0.340	4.820	0.164		0.14		Stockholm						
19H-5, 110–111	174.605	201.935	199.09	262.80	38.477	–1.68	–114.11	1.20	0.327	5.144	0.168	0.03	0.03	63.2	BSU						
19H-5, 120–121	174.705	202.035	199.20	262.93	38.502	–1.68	–114.09	1.23	0.381	5.170	0.197		0.14		Stockholm						
19H-5, 130–131	174.805	202.135	199.29	263.03	38.506	–1.68	–114.09	1.21	0.350	6.215	0.218	0.04	0	61.7	BSU						
19H-5, 140–141	174.905	202.235	199.39	263.14	38.523	–1.68	–114.08	1.20	0.330	6.233	0.206		0.15		Stockholm						
19H-6, 0–1	175.005	202.335	199.50	263.27	38.544	–1.69	–114.06			6.254			0.18		Stockholm						
19H-6, 10–11	175.105	202.435	199.59	263.37	38.560	–1.69	–114.05	1.22	0.363	6.270	0.228	0.03	0.06	54.8	BSU						
19H-6, 20–21	175.205	202.535	199.70	263.49	38.580	–1.69	–114.04	1.19	0.325	6.289	0.204		0.15		Stockholm						
19H-6, 30–31	175.305	202.635	199.79	263.59	38.596	–1.70	–114.03	1.22	0.363	6.306	0.229	0.03	0.08	57.4	BSU						
19H-6, 40–41	175.405	202.735	199.89	263.71	38.615	–1.70	–114.02	1.21	0.351	6.325	0.222		0.13		Stockholm						
19H-6, 50–51	175.505	202.835	200.00	263.83	38.635	–1.70	–114.00	1.22	0.362	6.344	0.230	0.04	0	62.8	BSU						
19H-6, 60–61	175.605	202.935	200.09	263.93	38.651	–1.70	–113.99	1.23	0.377	6.360	0.240		0.17		Stockholm						
19H-6, 70–71	175.705	203.035	200.20	264.04	38.628	–1.70	–114.01	1.23	0.388	8.994	0.349	0.04	0.04	61.8	BSU						
19H-6, 80–81	175.805	203.135	200.29	264.13	38.638	–1.70	–114.00	1.22	0.367	9.004	0.330		0.14		Stockholm						
19H-6, 90–91	175.905	203.235	200.39	264.23	38.649	–1.70	–114.00	1.20	0.338	9.016	0.305	0.04	0	69.4	BSU						
19H-6, 100–101	176.005	203.335	200.50	264.34	38.661	–1.71	–113.99	1.21	0.347	9.028	0.313		0.15		Stockholm						
19H-6, 110–111	176.105	203.435	200.59	264.43	38.671	–1.71	–113.98	1.21	0.354	9.038	0.320	0.04	0.52	69.4	BSU						
19H-6, 120–121	176.205	203.535	200.70	264.54	38.684	–1.71	–113.97	1.23	0.391	9.050	0.354		6.93		Stockholm						
19H-6, 130–131	176.305	203.635	200.79	264.63	38.694	–1.71	–113.97	1.26	0.441	9.060	0.400	0.04	9.06	62.0	BSU						
19H-6, 140–141	176.405	203.735	200.89	264.73	38.705	–1.71	–113.96	1.25	0.424	9.071	0.385		11.72		Stockholm						
19H-7, 0–1	176.505	203.835	201.00	264.83	38.716	–1.72	–113.95			9.082			30.56		Stockholm						
19H-7, 10–11	176.605	203.935	201.09	264.92	38.720	–1.72	–113.95			8.723		0.03	31.35	44.3	BSU	10889	2.24	0.58	0.030	0.013	Stockholm
20H-1, 0–1	177.005	205.335	202.49	266.32	38.887	–1.75	–113.84			6.787			1.95		Stockholm						
20H-1, 10–11	177.105	205.435	202.59	266.41	38.912	–1.75	–113.82			6.561		0.04	6.97	57.2	BSU						
20H-1, 20–21	177.205	205.535	202.70	266.52	38.928	–1.75	–113.81	1.16	0.259	6.577	0.170		3.66		Stockholm						
20H-1, 30–31	177.305	205.635	202.79	266.61	38.942	–1.75	–113.80	1.17	0.286	6.591	0.189	0.04	1.42	58.7	BSU						
20H-1, 40–41	177.405	205.735	202.89	266.71	38.953	–1.76	–113.80	1.15	0.246	6.472	0.159		1.15		Stockholm						
20H-1, 50–51	177.505	205.835	203.00	266.82	38.970	–1.76	–113.79	1.18	0.304	6.489	0.197	0.03	4.93	55.6	BSU						
20H-1, 60–61	177.605	205.935	203.09	266.91	38.984	–1.76	–113.78	1.17	0.292	6.503	0.190		4.59		Stockholm						
20H-1, 70–71	177.705	206.035	203.20	267.02	39.001	–1.76	–113.77	1.16	0.273	6.520	0.178	0.04	0.1	58.1	BSU						

Notes: LSR = linear sedimentation rate, MAR = mass accumulation rate, PDB = Peedee Belemnite, BSU = Boise State University, Stockholm = Stockholm University. Only a portion of this table appears here. The complete table is available in **ASCII.**

Table T3. Carbonate events between 50 and 34 Ma observed at Sites 1218 and/or 1219.

Event	Site	Age of interval (Ma)	Depth (rmcd)	Magnetochron	Comments
CAE-1	1219	47.9–46.9	251.4–248.7	Top C20r	
CAE-2	1219	45.9–44.2	243.5–239.0	Middle C20n	
CAE-3	1219	42.2–40.7	228.7–218.8	Top C20n–middle C18r	Offset in age because of CCD
	1218	Top of basalt to 40.3	To 274.6	? to top C18r	
CAE-4	1219	39.3–38.6	205.1–199.8	C18n.1n	Offset in age because of CCD
	1218	39.9–38.2	272.6–261.6	C18n.2n–C18n.1n	
CAE-5	1218	37.7–37.4	259.6–257.7	Top C17n.2n–lower C17n.1n	
CAE-6	1218	36.5–36.1	253.8–251.5	C16n.2r–middle C16n.2n	
CAE-7	1218	35.4–34.6	248.4–245.4	Top C16n.1n–lower C13r	

Notes: CAE = carbonate accumulation event, rmcd = revised meters composite depth. CCD = carbonate compensation depth.

Table T4. Estimates of carbonate compensation depth through the Eocene. (**See table notes.** Continued on next two pages.)

Site 1218				Site 1219					
Interpolated age (Ma)	Interpolated average cm^3 MAR	Interpolated depth (rmcd)	Paleodepth (m)	Interpolated age (Ma)	Interpolated average MAR (cm^3)	Interpolated depth (rmcd)	Paleodepth (m)	Estimated CCD (m)	Site 1220 paleodepth (m)
33.9	0.116	242.12	3741						4307
34	0.01	242.98	3736						4304
34.1	0.024	243.55	3730						4301
34.2	0.031	243.92	3724						4297
34.3	0.016	244.29	3718						4294
34.4	0.02	244.66	3712						4291
34.5	0.019	245.03	3706						4287
34.6	0.013	245.39	3700						4284
34.7	0.017	245.68	3694						4280
34.8	0.017	245.96	3688						4277
34.9	0.034	246.24	3681						4273
35	0.033	246.55	3675						4270
35.1	0.019	246.89	3669						4266
35.2	0.027	247.30	3662						4262
35.3	0.074	247.78	3656						4259
35.4	0.081	248.35	3650						4255
35.5	0.014	248.93	3644						4252
35.6	0.001	249.30	3637					**3637**	4248
35.7	0.001	249.66	3630					**3630**	4245
35.8	0.009	250.02	3624						4241
35.9	0.013	250.38	3617						4238
36	0.028	250.95	3610						4235
36.1	0.168	251.53	3604						4231
36.2	0.222	252.10	3597						4228
36.3	0.185	252.68	3590						4224
36.4	0.118	253.25	3583						4221
36.5	0.059	253.83	3576						4217
36.6	0.047	254.37	3569						4214
36.7	0.062	254.78	3562						4210
36.8	0.047	255.19	3555						4206
36.9	0.021	255.60	3548						4203
37	0.022	256.02	3540						4199
37.1	0.042	256.43	3533						4195
37.2	0.02	256.85	3525						4191
37.3	0.031	257.26	3518						4188
37.4	0.045	257.68	3510						4184
37.5	0.1	258.27	3502						4181
37.6	0.184	258.96	3495						4177
37.7	0.123	259.55	3487						4173
37.8	0.057	259.88	3479						4169
37.9	0.058	260.26	3470						4166
38	0.06	260.79	3462						4162
38.1	0.054	261.20	3454	38.1	0.000	197.27	4080	*3508*	4158
38.2	0.031	261.61	3445	38.2	0.000	197.75	4076	*3476*	4154
38.3	0.075	262.04	3437	38.3	0.000	198.25	4072	*3512*	4150
38.4	0.192	262.47	3428	38.4	0.000	198.80	4069	*3620*	4147
38.5	0.176	263.01	3419	38.5	0.000	199.16	4065	*3595*	4143
38.6	0.441	263.82	3410	38.6	0.002	199.77	4061	**4064**	4139
38.7	0.717	264.74	3402	38.7	0.038	200.85	4058	**4095**	4135
38.8	0.412	265.69	3393	38.8	0.037	202.21	4055	**4120**	4132
38.9	0.313	266.35	3383	38.9	0.007	202.53	4051	**4066**	4128
39	0.331	267.03	3374	39	0.017	203.19	4047	**4083**	4124
39.1	0.218	267.59	3364	39.1	0.026	203.99	4043	**4135**	4120
39.2	0.219	268.01	3354	39.2	0.025	204.47	4039	**4127**	4117
39.3	0.201	268.68	3344	39.3	0.007	205.10	4036	**4061**	4113
39.4	0.113	269.18	3334	39.4	0.002	206.08	4032	**4045**	4109
39.5	0.06	269.59	3324	39.5	0.000	206.58	4028	*3380*	4105
39.6	0.043	270.33	3313	39.6	0.000	207.28	4025	*3360*	4101
39.7	0.043	271.10	3302	39.7	0.000	208.02	4021	*3350*	4098
39.8	0.046	271.90	3291	39.8	0.000	209.37	4017	*3340*	4094
39.9	0.028	272.62	3280	39.9	0.000	210.19	4014	*3310*	4090
40	0.005	273.23	3269	40	0.000	210.77	4010	*3270*	4087
40.1	0	273.97	3257	40.1	0.000	211.61	4006	**<3257**	4083
40.2	0.003	274.57	3244	40.2	0.000	212.19	4002	*3250*	4078
40.3	0.013	275.15	3232	40.3	0.000	212.60	3998	*3250*	4074
40.4	0.045	275.76	3219	40.4	0.000	213.08	3994	*3260*	4070

Table T4 (continued).

Site 1218				Site 1219					
Interpolated age (Ma)	Interpolated average cm^3 MAR	Interpolated depth (rmcd)	Paleodepth (m)	Interpolated age (Ma)	Interpolated average MAR (cm^3)	Interpolated depth (rmcd)	Paleodepth (m)	Estimated CCD (m)	Site 1220 paleodepth (m)
40.5	0.051	276.42	3205	40.5	0.000	213.75	3990	*3260*	4067
40.6	0.147	277.16	3191	40.6	0.000	214.41	3986	*3340*	4063
40.7	0.283	278.31	3177	40.7	0.009	215.42	3983	**4009**	4059
40.8	0.534	279.71	3163	40.8	0.080	216.88	3979	**4123**	4056
40.9	0.79	281.58	3148	40.9	0.232	218.76	3976	**4320**	4052
41	0.693	282.87	3132	41	0.234	219.98	3973	**4402**	4048
41.1	1.091	284.71	3116	41.1	0.210	220.92	3969	**4172**	4044
41.2	1.408	287.16	3099	41.2	0.242	222.72	3966	**4146**	4040
41.3	1.545	289.64	3081	41.3	0.252	223.64	3962	**4134**	4035
41.4	1.323	291.93	3061	41.4	0.250	225.02	3958	**4167**	4031
41.5	0.804	293.27	3039	41.5	0.125	225.98	3954	**4122**	4027
				41.6	0.022	226.43	3950	*3970*	4022
				41.7	0.027	226.58	3946	*3970*	4018
				41.8	0.032	226.83	3941	*3970*	4014
				41.9	0.029	227.14	3937	*3970*	4010
				42	0.019	227.66	3932	*3950*	4005
				42.1	0.019	228.17	3928	*3950*	4001
				42.2	0.013	228.68	3924	*3940*	3997
				42.3	0.005	229.20	3919	*3920*	3992
				42.4	0.011	229.71	3915	*3930*	3988
				42.5	0.015	230.23	3911	*3930*	3984
				42.6	0.007	230.74	3906	*3910*	3979
				42.7	0.004	231.25	3902	*3910*	3975
				42.8	0.010	231.76	3897	*3910*	3971
				42.9	0.013	232.28	3893	*3910*	3967
				43	0.015	232.79	3888	*3900*	3963
				43.1	0.016	233.39	3884	*3900*	3959
				43.2	0.010	233.95	3879	*3890*	3954
				43.3	0.004	234.33	3875	*3880*	3950
				43.4	0.002	234.85	3870	*3870*	3946
				43.5	0.001	235.36	3865		3942
				43.6	0.003	235.87	3861	*3860*	3937
				43.7	0.005	236.38	3856	*3860*	3933
				43.8	0.005	236.90	3851	*3860*	3929
				43.9	0.005	237.42	3847	*3850*	3924
				44	0.003	237.93	3842	*3850*	3920
				44.1	0.000	238.46	3837		3916
				44.2	0.013	238.95	3833	*3850*	3911
				44.3	0.052	239.47	3828	*3880*	3907
				44.4	0.072	239.99	3823	*3900*	3899
				44.5	0.071	240.49	3818	*3890*	3894
				44.6	0.089	241.01	3813	*3900*	3890
				44.7	0.046	241.51	3808	*3850*	3885
				44.8	0.020	242.04	3803	*3820*	3881
				44.9	0.016	242.55	3798	*3810*	3876
				45	0.025	243.05	3793	*3820*	3872
				45.1	0.033	243.51	3788	*3820*	3867
				45.2	0.053	243.95	3783	*3840*	3863
				45.3	0.073	244.34	3778	*3850*	3858
				45.4	0.073	244.63	3773	*3850*	3853
				45.5	0.036	244.91	3767	*3800*	3848
				45.6	0.004	245.18	3762	*3770*	3843
				45.7	0.009	245.45	3757	*3770*	3838
				45.8	0.016	245.73	3751	*3770*	3833
				45.9	0.010	246.00	3746	*3760*	3828
				46	0.001	246.27	3740		3823
				46.1	0.000	246.54	3735		3819
				46.2	0.000	246.81	3729		3814
				46.3	0.001	247.09	3724		3809
				46.4	0.001	247.36	3718		3804
				46.5	0.001	247.64	3712		3799
				46.6	0.002	247.90	3707	*3710*	3794
				46.7	0.001	248.18	3701		3789
				46.8	0.001	248.45	3695		3784
				46.9	0.004	248.72	3689	*3690*	3778
				47	0.012	249.00	3684	*3700*	3773
				47.1	0.024	249.26	3678	*3700*	3768

Table T4 (continued).

Site 1218				Site 1219					
Interpolated age (Ma)	Interpolated average cm^3 MAR	Interpolated depth (rmcd)	Paleodepth (m)	Interpolated age (Ma)	Interpolated average MAR (cm^3)	Interpolated depth (rmcd)	Paleodepth (m)	Estimated CCD (m)	Site 1220 paleodepth (m)
				47.2	0.017	249.54	3672	*3690*	3763
				47.3	0.007	249.81	3666	*3670*	3758
				47.4	0.009	250.08	3660	*3670*	3752
				47.5	0.009	250.36	3654	*3660*	3747
				47.6	0.010	250.63	3648	*3660*	3742
				47.7	0.010	250.90	3642	*3650*	3736
				47.8	0.008	251.17	3635	*3640*	3731
				47.9	0.003	251.44	3629	*3630*	3725
				48	0.001	251.72	3623		3720
				48.1	0.001	252.00	3616		3714
				48.2	0.001	252.26	3610		3708
				48.3	0.001	252.53	3604		3703
				48.4	0.001	252.81	3597		3697
				48.5	0.001	253.08	3591		3691
				48.6	0.000	253.35	3584		3686
				48.7	0.000	253.62	3577		3680
				48.8	0.000	253.90	3571		3674
				48.9	0.000	254.17	3564		3668
				49	0.000	254.44	3557		3662
				49.1	0.000	254.72	3550		3656
				49.2	0.000	254.99	3543		3650
				49.3	0.000	255.26	3536		3644
				49.4	0.000	255.53	3529		3637
				49.5	0.000	255.80	3522		3631
				49.6	0.000	256.08	3514		3625
				49.7	0.000	256.35	3507		3618
				49.8	0.000	256.62	3500		3612
				49.9	0.000	256.89	3492		3605

Notes: Mass accumulation rates (MARs) are averaged over 100-k.y. intervals. Carbonate compensation depth (CCD) estimates in plain text are one-site estimates assuming 0.001 $g/cm^2/k.y.$ loss of $CaCO_3$ per additional meter of water depth. CCD estimates in bold text are estimates using both Sites 1218 and 1219. CCD estimates in italics are extrapolations of the CCD assuming a decrease of roughly 0.001 g $CaCO_3/cm^2/k.y.$ per additional meter of water depth near the CCD.